FEATURE ARTICLE

Interfacial Charge Carrier Dynamics of Colloidal Semiconductor Nanoparticles

Jin Z. Zhang

Department of Chemistry, University of California, Santa Cruz, California 95064

Received: February 14, 2000; In Final Form: April 14, 2000

Understanding the dynamic properties of charge carriers at the liquid−semiconductor interface is critical to many applications including photocatalysis, solar energy conversion and photoelectrochemistry. Dynamic properties of charge carriers, including trapping, recombination, and transfer, in a number of semiconductor nanoparticle systems have been studied using powerful time-resolved laser techniques. Several interesting features have been identified, including exciton−exciton annihilation upon trap state saturation at high excitation intensities for CdS, CdSe, TiO_2, ultrafast electron injection in dye sensitization of TiO_2, increased transient absorption over transient bleach with increasing intensity for Ag_2S and Cu_xS due to trap state saturation, surface dependence of electronic relaxation in PbI_2 and BiI_3, complex kinetics of the orange emission in Mn-doped ZnS, and surface-independent relaxation for Fe_2O_3 and PbS. These observations provide new insight into the interfacial charge carrier properties in colloidal semiconductor nanoparticles, which is important for designing novel nanoarchitectures for emerging technologies.

Introduction

Nanoparticles (NPs) refer to a class of materials with relevant physical dimensions on the length scale of a few to a few hundred nanometers. Both equilibrium and dynamic properties of nanomaterials can be very different from those of their corresponding bulk materials or isolated atoms and molecules.[1−19,20] Their properties are often strongly dependent on the particle size, shape, and surface properties. It is fundamentally interesting to understand how properties of nanoparticles vary with these parameters. For example, spatial confinement is expected to lead to changes in the density of states (DOS) for both electrons and phonons and the mechanisms and rates of electron−hole recombination. The possibility to control the properties of nanoparticles by varying these parameters is significant to many technological applications, ranging from microelectronics to nonlinear optics, optoelectronics, catalysis, and photoelectrochemistry. For instance, the color and redox potential of semiconductor nanoparticles can be tuned by changing particle size. This can be very useful for applications in optics, nonlinear optics, and photocatalysis.[6,7] The possibility of forming surperlattices from NPs presents a whole new class of nanomaterials for photonics and other applications.

There are many interesting examples demonstrating the unique properties and their applications of semiconductor nanoparticles as well as their dependence on particle size, shape, and surface characteristics. The most notable size effect is the significant blue shift of electronic absorption and emission spectra with decreasing size due to quantum confinement, especially when the particle size is smaller than the Bohr exciton radius.[1−4,6,8−15] The refractive index and nonlinear optical properties of nanoparticles have also been predicted and found to change significantly compared to those of bulk.[10,21] The metling temperature of nanoparticles, e.g. CdS, strongly depends on particle size and is substantially lower than the bulk melting temperature.[22] The thermodynamics and kinetics of first-order solid-state phase transitions are altered in nanoparticles as compared to bulk for CdSe.[23] Fabrication of devices such as single electron transistor,[24] light emitting diodes,[25] solar cells,[26] and sensors[27] based on semiconductor nanoparticles has been explored and tested. The strong size-dependent fluorescence, in conjunction with ease of coupling to biological molecules such as proteins and DNA, promises for applications in biological fluorescence imaging.[28,29] Semiconductor nanoparticles also show potential as photonic band gap materials.[30] New applications are expected to emerge as the properties of nanoparticles are better characterized and understood.

One complication involved with the study of nanoparticles is that the various parameters are not all independent. It is thus often challenging to study the dependence of the materials properties on a single parameter. For example, as the particle size decreases, the surface-to-volume (S/V) ratio increases and the particle shape can also change. However, with careful control of synthesis conditions, in many cases it is possible to obtain high quality samples that allow investigation of the dependence of the nanoparticle properties on some of the parameters.

Nanoparticles have been the subject of research for many decades. Recently, nanomaterials have received considerable renewed attention because of their promise in many current and potential applications. Properties of nanoparticles have been characterized using a variety of techniques including spectroscopy, microscopy, and X-ray techniques. Most studies have focused on their equilibrium properties, such as optical absorption and emission, particle shape, surface structure, interparticle interaction, self-assembly, and formation of superlattices.[13,19,31−35]

Direct study of the dynamic properties of charge carriers in nanoparticles is relatively new. Dynamic studies not only help

10.1021/jp000594s CCC: $19.00
Published on Web 06/23/2000

to gain important fundamental insight into the charge carrier properties but also provide complementary information to equilibrium studies, since dynamic properties are intimately coupled with equilibrium properties. For instance, electronic relaxation reflects interaction of the electron with phonons, surfaces, and other charge carriers. Most dynamic studies have been performed using time-resolved laser spectroscopic techniques. In this article, I will provide an overview of some of the recent studies of dynamics properties of semiconductor nanoparticles. The first part of the article will cover experimental techniques for synthesis and characterization of semiconductor nanoparticles. I will concentrate on nanoparticle systems whose dynamic properties have been studied. The discussion of experimental techniques will focus on time-resolved laser spectroscopy, which is the primary technique used for dynamic studies. The second part of the article will discuss dynamics of a number of important examples of semiconductor nanoparticle systems in some detail, including CdS, PbS, Cu_xS, Ag_2S, AgI, PbI_2, BiI_3, TiO_2, Fe_2O_3, ZnO, Mn-doped ZnS, and Si. I will concentrate on examination of possible dependence of charge carrier dynamics on parameters such as particle size, surface, and shape. Comparison and contrast will be made between different nanoparticle systems. A summary will be given at the end of the article.

Experimental Techniques

Synthesis of Semiconductor Nanoparticles. There are many different ways to make semiconductor nanoparticles. Detailed discussions of synthetic methods are unnecessary here and can be found in many of the references cited. I will mention only examples of nanoparticle synthesis that are relevant to this article. Colloidal semiconductor nanoparticles are usually prepared based on wet chemistry methods by arrested precipitation from homogeneous solutions by controlled release of ions or forced hydrolysis in the presence of surfactants. Surfactants or stabilizers are often used to stabilize NPs by stopping or controlling the crystal growth following nucleation, since, otherwise, NPs are thermodynamically unstable and tend to coalesce and grow to large size or bulk crystals.[36−40] In some cases, the stabilization is carried out by ions or charges on the surface of the NPs.

A number of metal chalcogenide semiconductor NPs can be easily prepared using colloidal chemistry methods. For example, CdS can be synthesized by controlled mixing of Cd^{2+} with sulfide ions in the presence of surfactants.[40,41] To passivate the surface of NPs for removing surface defects and controlling surface properties, organic or biological molecules can be used, e.g., TOPO (tri-*n*-octylphosphine oxide) used for CdS and CdSe[42,43] and cysteine and glutathione for CdS and ZnS.[44,45] Passivation of surface defects often leads to enhanced photoluminescence.[36,46] ZnS and CdSe NPs can be synthesized using techniques similar to those used for CdS.[47] Mixed or doped colloidal particles such as $Zn_xCd_{1-x}S$ or Mn-doped ZnS can be prepared by mixing the desired metal ions as the starting material in synthesis.[46,48] Mn-doped ZnS can also be synthesized in reverse micelles.[49] PbS NPs can be prepared from reaction of $Pb(NO_3)_2$ with H_2S in the presence of surfactant polymers such as poly(vinyl alcohol) (PVA).[50,51] Cu_xS ($x = 1$ to 2) can be synthesized using stabilizers such as poly(ethylene glycol) (PEG),[52] poly(vinylpyrrolidone) (PVP), bovine serum albumin (BSA), or casein hydrolysate-enzymatic (CAS).[53] NPs of MoS_2, a layered semiconductor, have be prepared using inverse micelle methods.[54,55] Ag_2S NPs capped with cysteine and glutathione can be prepared by first forming complexes between silver ions and cysteine or glutathione and then reacting with sulfide ions.[56]

Metal oxide NPs can be prepared using similar wet colloidal chemistry techniques. For instance, TiO_2 can be prepared by hydrolyzing Ti(IV) salt, e.g., $TiCl_4$[57] or Ti(IV) tetraisopropoxide.[58,59] γ-Fe_2O_3 NPs can be synthesized by selective reaction and oxidation of Fe^{2+} and Fe^{3+} ions.[60,61] α-Fe_2O_3 NPs can be prepared by hydrolysis of Fe^{3+}.[62,61] ZnO colloidal particles can be prepared in a similar manner.[63] Colloidal particles of SnO_2, TiO_2, and Fe_2O_3 are also commercially available.

Several metal iodide semiconductors can be prepared conveniently. PbI_2 NPs can be prepared based on reaction between $Pb(NO_3)_2$ and KI in organic solvents such as alcohols and acetonitrile.[64,65] In water, a surfactant such as poly(vinyl alcohol) is needed for making PbI_2 NPs.[65,66] AgI can be prepared by reacting NaI with $Ag(NO_3)$ in the presence of a stabilizing polymer such as poly(*N*-vinylpyrrolidone).[67,68] BiI_3 can be prepared similarly, except that nitric acid has to be added to enhance the solubility of the Bi^{3+} salt.[69]

Preparation of Si NPs is more involved,[70−78] and there are no simple wet chemistry methods available for making Si NPs at this point. In general, colloidal nanoparticles of semiconductors with more covalent chemical bonding are more difficult to make than those with ionic bonding.[20]

Characterization of Nanoparticles. The characterization of nanoparticles involves various microscopic, spectroscopic, and X-ray techniques. Microscopic techniques such as transmission electron microscopy (TEM), scanning tunneling microscopy (STM), and atomic force microscopy (AFM) are the most direct methods for determining particle size and shape.[13,16,79,80] With high resolution microscopy such as HRTEM, particle shape, crystal lattice structures, and grain boundaries of nanoparticles can be clearly determined, as shown for PbS (A), Ag_2S (B), and PbI_2 (D) nanoparticles in Figure 1. With high-resolution microscopy, it is found that most nanoparticles are not spherical but are formed in different interesting shapes such as cubes, prisms, or needles, often with well-defined facets (Figure 1).[13,81−83] For example, α-Fe_2O_3 nanoparticles are mostly formed in spindle-shapes, as shown in Figure 1C. The shapes of particles are sensitive to the preparation methods and conditions, e.g., reaction temperature and surfactants used to stabilize the particles. Surface properties of NPs have been studied using various types of spectroscopy, such as electronic absorption,[84,85] fluorescence,[40,46,80,86] IR,[65] and Raman.[43] These spectroscopic techniques are very useful in characterizing structural, optical, and electronic properties of nanoparticles. Fluorescence spectroscopy is especially sensitive to the electronic properties of surface trap states that are usually difficult to examine by other methods. Raman and IR are sensitive to lattice structure and species adsorbed on the particle surface. In addition, X-ray diffraction,[23,87,88] X-ray absorption, and photoemission techniques[89] have also been employed to characterize nanoparticles. In particular, X-ray absorption fine structure (XAFS) measurements have been found useful in determining local and surface structures of NPs, as demonstrated successfully for TiO_2[90] and CdTe.[91] Small-angle X-ray scattering is also useful for determining particle size, especially for very small particles that may not be stable for TEM measurements, e.g. Mn-doped ZnS.[49]

Dynamics Measurements with Time-Resolved Techniques. For measurements of charge carrier dynamics in nanoparticles, time-resolved laser techniques, including transient absorption, transient bleach, and time-resolved fluorescence, have been employed. The basic approach is to first excite the nanoparticles with a short femtosecond or picosecond light pulse generated from an ultrafast laser system. In transient absorption, the excited charge carriers are then monitored with a second laser pulse

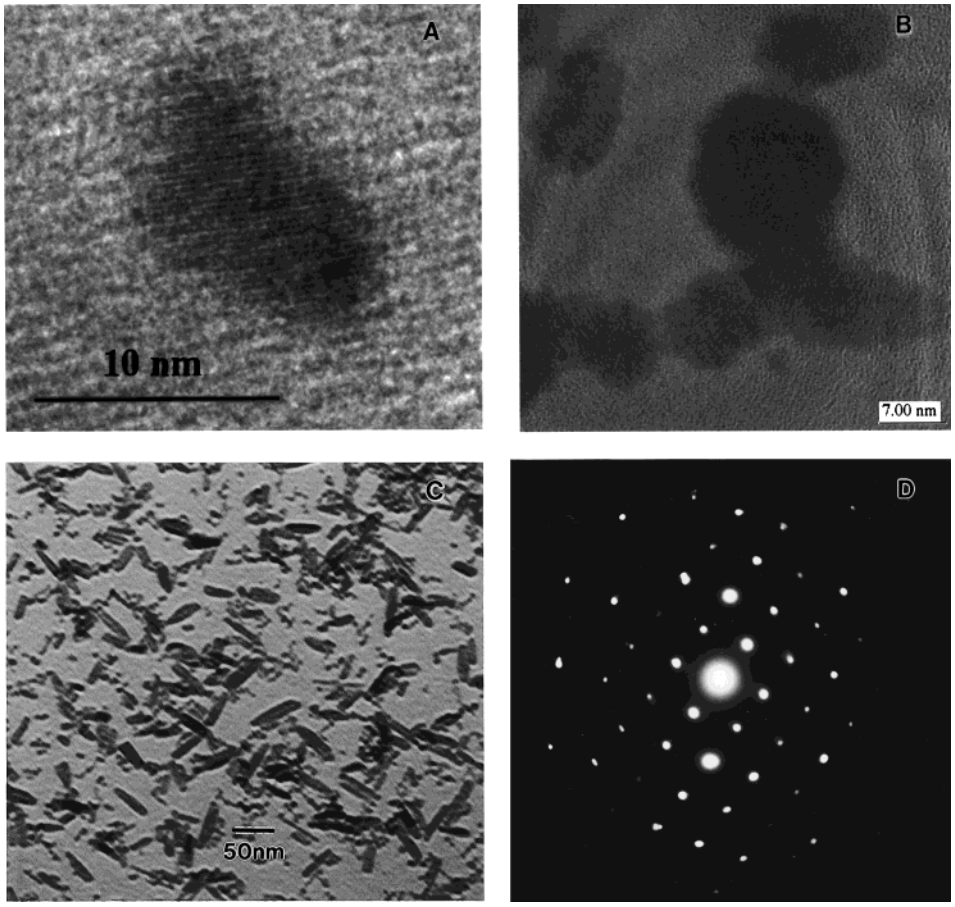

Figure 1. High-resolution transmission electron microscopy (HRTEM) images of PbS (A) and Ag_2S (B) NPs. (C) TEM image of α-Fe_2O_3 NPs. (D) High-resolution electron diffraction pattern of a single PbI_2 NP.

that is delayed with respect to the excitation (pump) pulse. The change in absorption of the second (probe) pulse reflects change in excited-state charge carrier population.[85] Alternatively, the ground-state population can be monitored as a transient bleach signal, which indicates depletion and recovery of the ground-state population.[92,93] Another method to monitor excited-state population is to time-resolve the luminescence from the excited state by using a fluorescence up-conversion method[94] or by using stimulated emission.[95] This technique is mainly useful for luminescent nanoparticles. A schematic diagram of a typical laser setup used for time-resolved measurements is shown in Figure 2. In the system used in our lab, femtosecond laser pulses generated from a Ti-sapphire oscillator are amplified in a Ti-sapphire regenerative amplifier.[85] The final output (500 μJ/pulse, 150 fs) centered at 780 nm is doubled in a KDP crystal to yield 390 nm pulses (30 μJ/pulse), which are used to excite the sample. The remaining 780 nm light following doubling is used to generate a white light continuum (500−950 nm) in a quartz or sapphire window, from which a single wavelength can be selected as a probe pulse to interrogate the excited-state population. The time delay between the probe and pump pulses can be varied with a delay line, e.g., a translation stage. The excited-state dynamics can be monitored by measuring changes of absorbance of the probe pulse as a function of delay time between the pump and probe. To obtain multiwavelength spectra, the white light can be used as a probe and dispersed after the sample with multiwavlength detectors such CCD or dual diode array detectors.

The excited-state population can also be monitored by detecting fluorescence following excitation. To time resolve the fluorescence on the ultrafast time scales requires special techniques such as fluorescence up-conversion. In this method, fluorescence is mixed with a "gating" pulse in a nonlinear optical crystal to generate an up-converted signal and the gating pulse is time-delayed with respect to the excitation pulse. The up-converted signal, with frequency equal to the sum of the gating pulse frequency and fluorescence frequency, is linearly proportional to the fluorescence intensity and contains dynamic information about the emitting species.[94] This can provide femtosecond time resolution, however, the signal is expected to be weak due to the typically low luminescence yield of nanoparticles. So far, no studies have been reported on the use of fluorescence up-conversion to study charge carrier dynamics in nanoparticles on the fs time scale. But it is anticipated that such experiments will be conducted in the future, since it is an excellent way to directly probe different trap states versus bandedge states. This is because the wavelength of emission of the bandedge states is different from that of trap states. By selecting the emission wavelength being up-converted, one can unambiguously determine dynamics of the emitting states. The recent advent of OPA (optical parametric amplifier) technology has made it easy to generate tunable excitation wavelengths from laser systems such as the one shown in Figure 2. Tunable excitation wavelength is desirable for studying samples absorbing at different wavelengths.

Interfacial Dynamic Properties of Charge Carriers in Semiconductor Nanoparticles. *Theoretical Considerations.* Semiconductors are generally divided into two classes: direct and indirect band gap according to their electronic band structures. Optical absorption and emission as well as electronic properties of these two types of semiconductors can be very different. For direct band gap semiconductors, electronic transi-

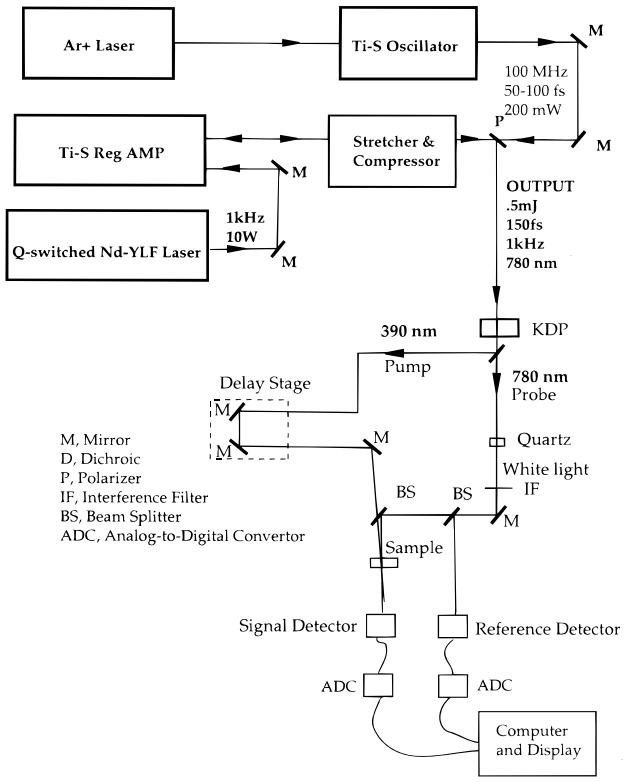

Figure 2. Schematic illustration of a femtosecond Ti-sapphire laser system used for transient absorption measurements. The abbreviations used are: Ti−S Oscillator for Ti-sapphire oscillator, Ti−S Reg AMP for Ti-sapphire regenerative amplifier, KDP for potassium dihydrogen phosphate.

tions from the valence band to the conduction band is electrical dipole allowed and the electronic absorption as well as emission are usually strong. For indirect band gap semiconductors, the valence band to conduction band electronic transition is electrical dipole forbidden and the transition is phonon assisted, i.e., both energy and momentum of the electron−hole pair are changed in the transition.[96] Both their absorption and emission are weaker compared to those of direct band gap semiconductors. Figure 3 shows a comparison of the electronic absorption and emission spectra of CdS, a direct band gap semiconductor, and Si, an indirect band gap material. The absorption peak near 430 nm for one of the CdS NP samples is known as the exciton peak. Such excitonic features are absent in indirect band gap semiconductor materials such as silicon.

For NPs of semiconductors, quantum confinement plays an important role in their electronic and optical properties. The quantum confinement effect can be qualitatively explained using the effective mass approximation.[1−3,9,97] For a spherical particle with radius R, the effective band gap, $E_{g,eff}(R)$, is given by

$$E_{g,eff}(R) = E_g(\infty) + \frac{\hbar^2\pi^2}{2R^2}\left(\frac{1}{m_e} + \frac{1}{m_h}\right) - \frac{1.8e^2}{\epsilon R} \qquad (1)$$

where $E_g(\infty)$ is the bulk band gap, m_e and m_h are the effective masses of the electron and hole, and ϵ is the bulk optical dielectric constant or relative permittivity. The second term on the right-hand side shows that the effective band gap is inversely proportional to R^2 and increases as size decreases. On the other hand, the third term shows that the band gap energy decreases with decreasing R due to the increased Coulombic interaction. The second term becomes dominant with small R, thus the effective band gap is expected to increase with decreasing R.

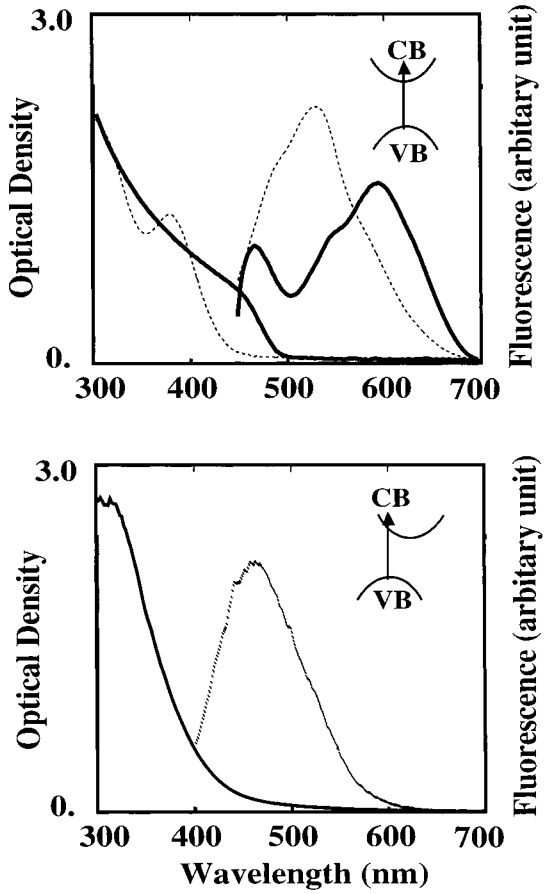

Figure 3. Comparison of electronic absorption (left) and fluorescence (right) spectra of NPs of CdS (top), a direct band gap, and Si (bottom), an indirect band gap, semiconductor. The fluorescence spectra were collected with excitation at 390 nm. Two different sized CdS samples are shown. One sample, capped with cysteine, has a smaller average size (1 nm) and blue-shifted exciton absorption peak. The other sample, capped with glutathione, has a larger average size (3 nm) and redder exciton absorption. The difference in band structure in momentum space representation is shown schematically in the inset.

The quantum size confinement effect becomes significant especially when the particle size becomes comparable to or smaller than the Bohr exciton radius, a_B, which is given by

$$a_B = \epsilon_0\epsilon h^2/\pi\mu e^2 \qquad (2)$$

where ϵ_0 and ϵ are the permittivity of vacuum and relative permittivity of the semiconductor, μ is the reduced mass of the electron and hole, $m_e m_h/(m_e + m_h)$, and e is the electron charge. The Bohr radius of CdS is around 2.4 nm,[7] and particles with radius smaller or comparable to 2.4 nm show strong quantum confinement effects as indicated by a significant blue shift of their optical absorption relative to that of bulk.[40,41,85] For example, the CdS NP sample with a smaller average size (1 nm) showed a substantially blue-shifted absorption spectrum compared to the sample with larger average size (2.5 nm), as shown in Figure 3 (top). The emission and absorption spectra of the two samples are clearly different.

The study of dynamic properties of charge carriers in semiconductor nanoparticles has received considerable attention in recent years. Issues of interest include charge carrier transfer, recombination, trapping, carrier−carrier interaction, and their dependence on particle size, shape, surface characteristics. Systems that have been studied include CdS, CdSe, PbS, CuS, Ag_2S, TiO_2, ZnO, Fe_2O_3, AgI, PbI_2, Si, MoS_2, BiI_3, and coupled

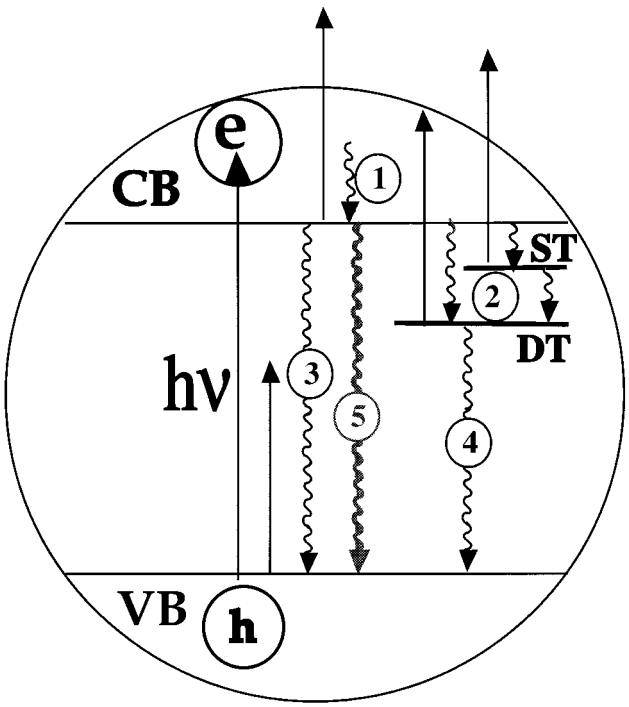

Figure 4. Schematic illustration of charge carrier relaxation in semiconductor NPs and the pump−probe scheme for monitoring the carrier dynamics. The long solid line with upward arrow indicates excitation and the short solid lines with upward arrows indicate probe of the conduction band, shallow and deep trap states, and valence band, respectively. The curved lines with downward arrows indicate different relaxation processes: (1) electronic relaxation within the conduction band, (2) trapping into shallow trap (ST) and deep trap (DT) states and further trapping from ST to DP, (3) bandedge electron−hole recombination, (4) trapped electron−hole recombination, and (5) exciton−exciton annihilation.

colloids such as CdS/TiO_2[98] or core/shell structures such as CdS/HgS.[93] In almost all of these systems, the dynamics of photogenerated charge carriers appear to be dominated by trapping and subsequent recombination of trapped carriers caused by a high density of surface trap states. Figure 4 shows schematically the major pathways for charge carrier relaxation following above band gap photoexcitation. The first step of relaxation should be electronic relaxation in the conduction band and hole relaxation in the valence band. This is mainly due to electron−phonon interaction and is expected to be on the time scale of 100 fs or less. Once the electron is relaxed to the bottom of the conduction and the hole to the top of the valence band, they can recombine radiatively or nonradiatively. If there are few or no band gap states, the recombination should be primarily radiative, i.e., strong bandedge luminescence should be observed, and the lifetime should be on the order of nanoseconds or longer. When states are present within the band gap due to surface or internal defects, they act to trap the charge carriers on time scales faster than radiative recombination, typically a few picoseconds to tens of picoseconds. Further trapping from shallow trap states to deep trap states can take place on the tens of ps to hundreds of ps time scales. The trapped charge carriers can recombine nonradiatively or radiatively, producing trap state emission that is red shifted with respect to bandedge emission. The trap states have lifetimes on the time scale from tens of picoseconds to nanoseconds or microsecond or even longer, depending on the nature of the trap states. The trap states also vary significantly in their energy levels or trap depth, which in turn determines how fast the trapping occurs and how long the trap states live. It should also be pointed out that the excitonic state, formed as a result of Coulombic interaction between the electron and hole, usually lies slightly below the bottom of the conduction band (few tens of meV) but above the trap states. This excitonic state can also be populated during the relaxation process. However, since the binding energy of the exciton is typically small, e.g., 30 meV for CdS, it is generally difficult to experimentally distinguish between the bottom of the conduction band and the excitonic state. We will simply refer to them as bandedge states.

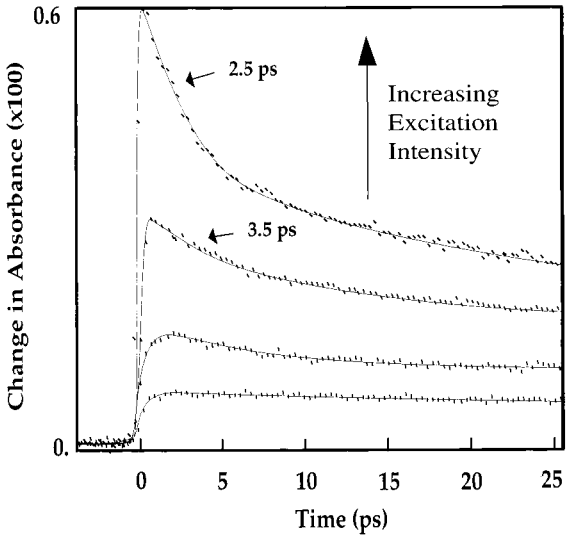

Figure 5. Excitation intensity dependent photoinduced electron relaxation dynamics of CdS NPs probed at 780 nm, following excitation at 390 nm. The fast decay component increases nonlinearly with excitation intensity and is absent at low intensity.

In terms of direct experimental probes of the excited charge carrier dynamics, three major techniques based on time-resolved laser spectroscopy have been used, including transient absorption, transient bleaching, and time-resolved fluorescence. These techniques have been described earlier in the Experimental Section. The following sections present several specific examples to illustrate how time-resolved experiments can be used to investigate the relaxation pathways of charge carriers in semiconductor nanoparticles. We will attempt to examine how the charge carrier dynamics depend on various parameters such as surface, size, and shape of nanoparticles.

CdS, CdSe, and Related Systems. CdS is among the most extensively studied semiconductor nanoparticle systems. Earlier dynamics studies on the picosecond time scale identified a strong transient bleach feature near the excitonic absorption region of the spectrum.[99−105] It was noticed that the peak of the bleach feature shifts with time, and one explanation proposed was increased screening by charge carriers for the particles.[106] It was also observed that there is a red shift of the transient absorption features in CdSe, which was explained by some as a result of formation of biexcitons.[107,108] Later, femtosecond measurements were carried out and a power dependence of the bleach recovery time was found for CdS.[92] The bleach recovery follows a double exponential rise with the fast component increasing with power faster than the slower component. Recent work from our lab using transient absorption found a similar power dependence of the electronic relaxation dynamics featuring a double exponential decay behavior with a fast (2−3 ps) and slow (50 ps) decay components.[46,85,109] As shown in Figure 5, the amplitude of the fast decay component increases with excitation intensity faster than that of the slow component. It grows nonlinearly, slightly subquadratic, with excitation intensity. This nonlinear fast decay was first attributed to nongeminate electron−hole recombination at high excitation intensities.[85] We

have subsequently carried out a more detailed investigation using fs transient absorption in conjunction with ns time-resolved fluorescence and found that the bandedge fluorescence was also power dependent.[46] These results led us to propose that the fast decay is due to exciton−exciton annihilation upon trap state saturation, as suggested previously,[110] and the slow decay is due to trapped charge carrier recombination. Therefore, the transient absorption signal observed has contributions from both bandedge electrons (excitons) and trapped electrons. At early times, the bandedge electrons have significant contribution, especially when trap states are saturated at high excitation intensities, while as time progresses the contribution from trapped electrons becomes more dominant. On long time scales (hundreds of ps to ns), the signal is essentially all from trapped charge carriers. We believe that this is true to many other colloidal semiconductor nanoparticles.[18,61,65,68,83] Our very recent study of the emission lifetime on the ns time scale of surface passivated and unpassivated CdS nanoparticles showed that the passivated sample with a lower density of surface trap states has a lower excitation threshold for observing exciton−exciton annihilation compared to the unpassivated sample.[111] This supports the model of exciton−exciton annihilation upon trap state saturation at high excitation intensities.[46]

One important issue involved in charge carrier relaxation in semiconductor NPs is the charge carrier trapping rate. For CdS NPs, an electron trapping time constant of about 100 fs has been suggested.[85,112] A longer trapping time (0.5−8 ps) was deduced for CdSe NPs based on time-resolved photon echo experiment.[113] An even longer trapping time of 30 ps has been reported for CdS NPs based on measurement of trap state emission.[38,114] A similar 30 ps electron trapping time for CdS NPs has been reported based on study of the effects of adsorption of electron acceptors such as viologen derivatives on the particle surface.[115] The hole trapping was found to be faster, a 1 ps hole trapping time has been reported for CdS based on time-resolved photoluminescence measurements.[114] The difference in trapping times reported could be either due to a difference in the samples used or different interpretations of the data obtained. It can be concluded, however, that the trapping time is on the order of a few hundred fs to tens of ps, depending on the nature of the NPs and quality of the sample. The trapping time may also be different for shallow traps and deep traps or further trapping from shallow traps to deep traps.

Charge-transfer dynamics from CdS and CdSe NPs to electron acceptors, e.g., viologen derivatives, adsorbed on the particle surface have been studied using transient absorption, transient bleach, and time-resolved fluorescence.[115,116] Electron transfer was found to take place on the time scale of 200−300 fs and competes efficiently with trapping and electron−hole recombination. These results are important to understanding interfacial charge transfer involved in photocatalysis and photoelectrochemistry applications.

A number of important relevant studies have been conducted on high quality samples of CdSe to measure and assign their size-dependent optical spectrum.[117−119] The measurements of the absorption and emission spectra were carried out at low temperature (∼10 K) to reduce inhomogeneous spectral broadening due to thermal effect. These studies have shown that the size dependence of up to 10 excited states in the absorption spectra of CdSe nanocrystals can be successfully described by uncoupled multiband effective mass (MBEM) theory that includes valence band degeneracy but not coupling between the conduction and valence bands. The assignment of the states provides a foundation for discussion of electronic structure of semiconductor nanopartciles.[120] The MEBM theory has very recently been extended to include conduction band−valence band coupling and applied to describe the size-dependent electronic structure of InAs nanocrystals.[121] To date, no systematic studies have been reported on the temperature dependence of charge carrier dynamics in semiconductor nanoparticles on the ultrafast time scales. At low temperature, nonradiative relaxation pathways should be suppressed and radiative fluorescence quantum yield is usually enhanced. Since the nonradiative relaxation processes are typically faster than radiative processes, suppression of nonradiative pathways at low temperature is expected to result in longer lifetimes of the charge carriers or slower overall relaxation. This has been clearly demonstrated in the temperature-dependent emission lifetime observed for CdSe nanocrystals measured on the ns time scale.[122] Direct study of the temperature dependence of charge carrier dynamics on the ultrafast time scale will help to gain further insight into the electronic relaxation mechanisms in semiconductor nanoparticles, e.g., the rates of nonradiative trapping and trap state-mediated recombination.

Other Metal Sulfide Nanoparticles: PbS, Cu_xS, and Ag_2S. PbS NPs are another interesting system in that their particle shapes can be readily varied by controlling synthetic conditions.[50,83,123−125] Also, since the Bohr radius of PbS is relatively large, 18 nm, and its bulk band gap is small, 0.41 eV,[126] it is easy to prepare particles with size smaller than the Bohr radius that show strong quantum confinement effects and still absorb in the visible part of the spectrum. We have attempted to study the surface and shape dependence of electronic relaxation in different shaped PbS NPs. While it is possible to observe significant changes in the ground state electronic absorption spectrum when particle shapes are changed from mostly spherical to needle and cube shaped by changing the surface capping polymers, the electronic relaxation dynamics remain about the same for the apparently different shaped particles.[83] For all cases studied, including capping with poly(vinyl alcohol), poly(vinylpyrrolidone), gelatin, polystyrene, poly(methyl methacrylate), and DNA, the electronic relaxation was found to feature a double exponential decay with time constants of 1.2 and 45 ps that are independent of probe wavelength and excitation intensity. We attributed the shape independence to the dominance of the surface properties on the electronic relaxation. While the shapes are different, the different samples may have similar surface properties. Therefore, if the dynamics are dominated by the surface, change in shape may not affect the electronic relaxation dynamics substantially. To study the possible intrinsic effect of size or shape, the surface needs to be better controlled so that the relaxation is not dominated by the surface, which is a challenging problem. Another possible but less likely explanation is that the relaxation is dominated by internal defects or intrinsic electronic states; changes in surface capping therefore do not affect the relaxation noticeably.

Copper sulfides (Cu_xS, $x = 1-2$) are interesting due to their ability to form with various stoichiometries. The copper−sulfur system ranges between the chalcocite (Cu_2S) and covellite (CuS) phases with several stable and metastable phases of varying stoichiometry in between. Their complex structures and valence states result in some unique properties.[52,127−136] For example, covellite had been believed to exist in two forms, brown CuS and green CuS, with the latter having an additional absorption band in the IR.[52,129,133,135,136] Green CuS has been found to be the true crystalline form of covellite composed of 1/3 Cu(II) and 2/3 Cu(I).[52,127−129,131,132] Brown CuS has been characterized to be a poor crystalline or amorphous type of covellite, CuS,

composed entirely of Cu(I) not Cu(II).[127,129,132] However, Cu(I)S is then not stoichiometrically balanced and therefore the appropriate label should probably be amorphous Cu_2S.[53,127] It has been observed that the preparation of Cu_xS nanoparticles at 30 °C gives green crystalline CuS (strong IR absorption) with metallic properties, while preparation at 10 °C gives brown amorphous Cu_2S with semiconductor properties.[129] The difference was attributed to the brown sample being in a metastable state, whereas the green sample is the stable crystalline state of CuS. The nature of the IR band is a central issue in discussing the difference between the different types of Cu_xS samples.[52,127−136] In a study of CuS nanoparticles by Drummond et al., the IR band was found to disappear following reduction to Cu_2S via viologen and was therefore attributed to the presence of Cu(II).[52,127] In the picosecond studies by Artemyev et al.,[133,136] brown Cu_xS samples were converted to green by heating, resulting in the appearance of the IR band. The IR band was attributed to a state in the band gap due to surface oxidation, which lies 1 eV below the conduction band. It was believed that this new middle-gap state was occupied by electrons and thus has electron donor character. However, the model appeared to have some inconsistencies.[53]

We have very recently synthesized crystalline CuS and amorphous as well as crystalline Cu_2S nanoparticles utilizing different capping molecules including poly(ethylene glycol) (PEG), polyvinlypyrrolidone (PVP), casein hydrolysate-enzymatic (CAS), and bovine serum albumin (BSA). A series of spectroscopic and dynamics studies have been performed on these samples. The ground-state electronic absorption spectra of the Cu_xS nanoparticles show three distinct types of Cu_xS formed: a green type assigned as crystalline CuS, and two brown types assigned as crystalline Cu_2S and amorphous Cu_2S. The IR band can be seen in Figure 6A for the green crystalline CuS, which can be obtained by exposing the brown amorphous Cu_2S to air and heating. This seems to support the earlier suggestion that brown amorphous Cu_2S is a metastable form which may convert to the thermodynamically more stable form of crystalline CuS[127,129] and thus correlates the presence of Cu(II) to the IR band. The brown types exhibit a steady increase in absorption toward shorter wavelengths starting around 650 nm, while the green type shows the same steady increase in absorption but with an additional absorption band in the infrared. ESR measurements of free Cu(II) ions in solution for all samples show the presence of Cu(II) in the brown amorphous samples but not in the green or brown crystalline samples.[53] In the dynamics measurements (Figure 6B and C), a dominant fast decay component with a slower decay component was observed in both types of Cu_2S and was independent of excitation intensity, probe wavelength, and capping agent. The fast decay (1.1 ps) is assigned to charge carrier trapping at shallow trap sites, while the long decay (80 ps) component is assigned primarily to deep trapping. The dynamics of crystalline CuS showed interesting power dependence. At low excitation intensities a bleach, due to ground-state absorption of the probe, with a fast recovery (430 fs) followed by a long time offset was observed (Figure 6D). The fast recovery is due to carrier trapping, leading to an increase in transient absorption. The long time offset is assigned to relaxation from shallow to deep traps and further relaxation of charge carriers from deep traps. At high excitation intensities, a transient absorption signal with a 1.1 ps decay and a slow rise with a lifetime >1 ns was seen in crystalline CuS (Figure 6D). The power dependence of the crystalline CuS could be attributed to trap state saturation.[53] Based on a simple kinetic model developed to model the data

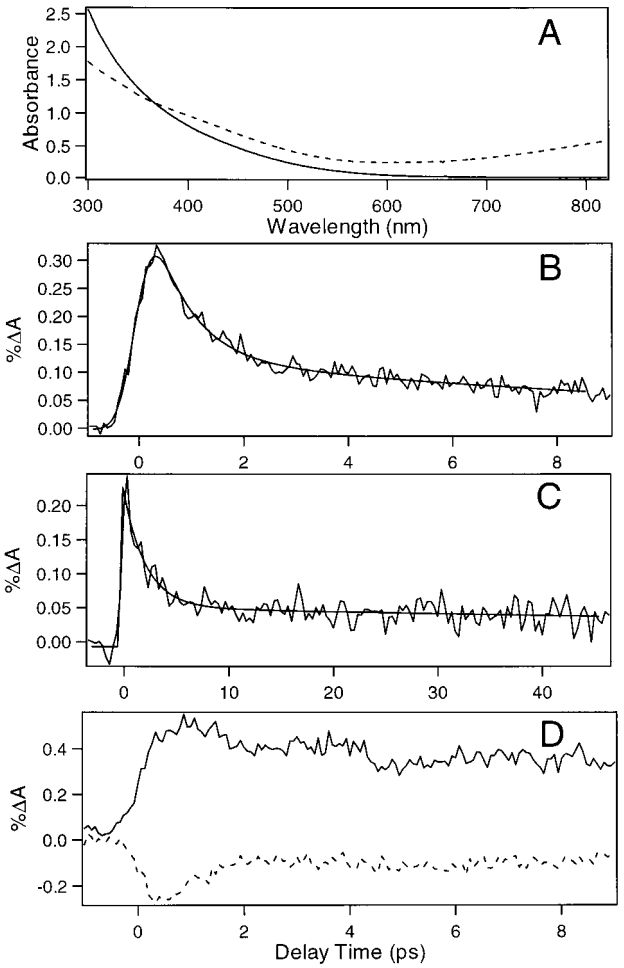

Figure 6. (A) Electronic absorption spectra of two Cu_xS nanoparticles: solid line for brown amorphous Cu_2S samples capped with PVP; dashed line for green crystalline CuS capped with PVP. (B) Transient absorption decay profiles of amorphous Cu_2S nanoparticles (PVP) on a short time scale probed at 790 nm following 390 nm excitation. (C) same as (B) except on a longer time scale. (D) Power dependent transient dynamics of green crystalline CuS (PVP) with excitation energy of 4 μJ/pulse (dashed line) and 12 μJ/pulse (solid line). The smooth solid lines are fits generated from a double exponential function with time constants of 1.1 and 80 ps.

for both Cu_2S and CuS, an alternative explanation was proposed for the middle-gap state, this state is an electron-acceptor state or unoccupied, and the IR absorption band corresponds to a transition from the valance band to this state.[53]

Ag_2S is potentially useful for photoimaging and photodetection in the IR region due to its strong absorption in the IR.[137] Ag_2S nanoparticles are usually difficult to synthesize due to their tendency to aggregate into bulk. One approach was to synthesize them in reverse micelles.[138] We have recently developed a new synthetic method for preparing Ag_2S nanoparticles using cysteine (Cys) and glutathione (GSH) as capping molecules and studied their optical and dynamic properties using spectroscopic and transient absorption techniques.[56] As shown in Figure 7, the ground-state electronic absorption spectra of the Ag_2S nanoparticles show a continuous increase in absorption cross section toward shorter wavelengths starting from the red (600−800 nm). For most of the nanoparticles studied, ultrafast dynamics of photoinduced electrons measured using femtosecond transient absorption/bleach spectroscopy feature a pulse-width limited (<150 fs) rise followed by a fast decay (750 fs) and a slower rise (4.5 ps), as shown in Figure 7B, C, and D.

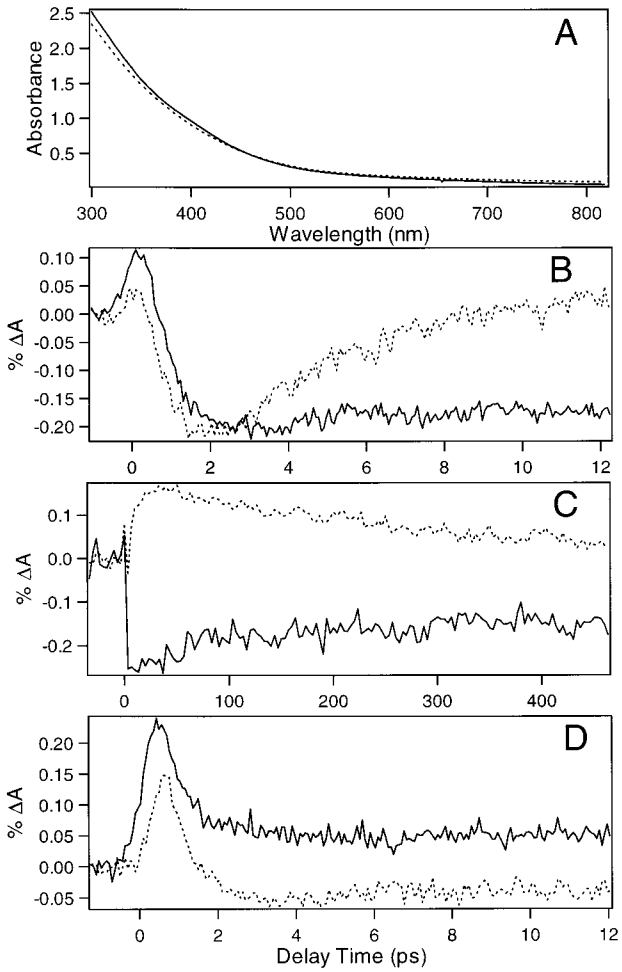

Figure 7. (A) Electronic absorption spectra of silver sulfide nanoparticles in water: solid line for GSH-1 and dotted line for Cys-1. (B) Time evolution of photoinduced electrons in GSH-1 (solid) and Cys-1 (dotted) on a short time scale, probed at 790 nm following excitation at 390 nm. (C) same as (B) except on a longer time scale. (D) Excitation intensity dependence of the electron relaxation dynamics of GSH-1 probed at 790 nm with excitation energy of 3.5 μJ/pulse (dotted) and 7 μJ/pulse (solid).

The signal has contributions from both transient absorption and transient bleach. On longer time scales, three (Cys-1, Cys-2, and GSH-2) of the four samples studied show a recovery with a 4.5 ps time constant that goes above the baseline and then decays gradually toward the baseline with a time constant of >1 ns. One sample (GSH-1) shows a bleach recovery that gradually approaches the baseline with a similar time constant (>1 ns) following the fast 4.5 ps rise. An interesting excitation intensity dependence was observed for all the samples: *the transient absorption contribution becomes more dominant over bleach with increasing excitation intensity*. Some representative data for two different intensities are shown in Figure 7D. A simple four-state kinetic model developed to account for the main features of the dynamics suggests that initial photoexcitation populates the conduction band and depletes the valence band within the laser pulse (<150 fs). The conduction band electrons are first trapped in shallow trap states with a time constant of 500 fs and then further trapped into deep traps with a constant of 4 ps. The deep trapped electrons finally recombine with the hole with a time constant of >1 ns. This model suggests that the difference in dynamics observed between the different samples is due to different absorption cross sections of deep trap states. The observed excitation intensity dependence of the dynamics is attributed to shallow trap state saturation at high intensities.

Mn-Doped ZnS. Mn^{2+}-doped ZnS is a novel system of interest because of its use as an important luminescent material. In this system, a small amount of Mn^{2+} is incorporated into the host ZnS nanocrystalline lattice. These particles possess interesting magnetic[139−142] and electro-optical properties.[143−147] As in bulk Mn^{2+} doped ZnS, the Mn^{2+} ion acts as a luminescence color center, emitting around 585 nm.[140,143,144,148−150] It has been claimed that the time scale for luminescence is shorter and the efficiency greater in the nanocrystalline system compared with bulk.[143,144] This is important because sensors, display devices, and lasers utilizing these nanoparticles are expected to be better performing due to rapid energy transfer to the Mn^{2+} ion, high saturation thresholds, and fast recombination arising from the Mn^{2+} color center imbedded in the nanocrystalline lattice. To explain the fast 20 ns decay, Bhargava et al. have proposed that, due to quantum confinement of the photogenerated charge carriers, there is a rehybridization between the s−p conduction band of the ZnS host and the 3d states of the Mn^{2+}. Given the strong coupling between donor and acceptor, there is a rapid energy transfer and consequent fast radiative decay. However, more recent work has thrown some doubt as to the true time scale for radiative energy relaxation.[151] Bol and Meijerink observed ns decay rates for the blue ZnS emission, but for the orange Mn^{2+} emission they observed a normal 1.9 ms decay time along with a small amplitude ns decay. Furthermore, in their system, the blue 420 nm emission band was observed to have a tail that extended into the orange Mn^{2+} region and could be observed with a 2 μs gate.[151] Thus Bol and Meijerink claimed that the fast ns decay observed by Bhargava et al. was due to ZnS trap state emission and not the Mn^{2+} emission. Unfortunately, the apparatus used in their experiment had limited time resolution (a 2 μs gate was used).

In our recent work we present new data to show that the time scale for the red emission centered around 585 nm does possess a large amplitude fast multiexponential decay with time constants of 250 ps, 7 ns, and 10 μs, in addition to a very slow decay with a time constant of 1.8 ms, similar to that observed in bulk.[49] The Mn^{2+}-doped ZnS NPs used in our study were prepared in reverse micelles, following a literature procedure[48,152] with some modification.[49] Figure 8A shows the UV−visible electronic absorption spectra of the doped (solid) and undoped (dashed) diluted ZnS nanoparticle suspension. The spectra feature a steep, excitonic absorption edge at 269 nm (doped) and 278 nm (undoped) typical of such systems, which are blue shifted relative to the 337 nm band gap of bulk ZnS as expected due to quantum confinement. This position of the excitonic absorption onset is similar to those reported by others on particles of similar size,[153] well within the quantum-confined region for ZnS possessing an exciton Bohr radius of 2.5 nm.[154] The results correlate to particles of 2.5 nm within the effective mass approximation.

Figure 8B shows the time-resolved emission results for the 585−640 nm orange emission usually associated with the Mn^{2+} dopant. Our data showed no wavelength dependence in contrast to previous work in the μs region.[145] The undoped sample showed a triple exponential decay with time constants of 250 ps, 7 ns, and 10 μs, while the doped sample possesses a 1.8 ms decay constant in addition to a fast triple exponential decay with time constants similar to those of the undoped sample. Since the fast triple exponential decay is present in both doped and undoped samples, it is attributed to trap state emission from ZnS. The 1.8 ms decay can only be attributed to Mn^{2+} in the

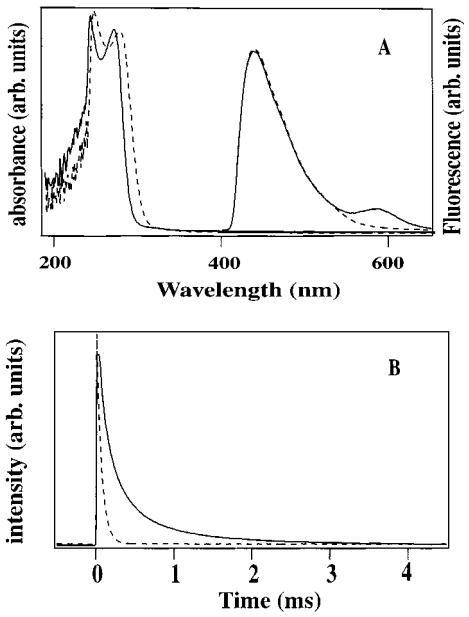

Figure 8. (A) Normalized absorption (right) and emission (left) spectra of doped (solid line) and undoped (dashed line) ZnS nanoclusters. (B) 600 nm emission intensity vs time collected using 285 nm excitation on the millisecond time scale (shorter time scale data not shown). On this time scale, the data for the doped clusters can be fit with a double exponential with a 10 μs fast component and a slower 1.8 ms component, while the undoped sample lacks the 1.8 ms decay component.

ZnS NPs. Therefore, both fast decays (250 ps, 7 ns, and 10 μs) and the 1.8 ms decay are observed in our data, and our results seem to partly support both of the earlier claims. However, it is most important to point out that our results seem to support the claim by Bol and Meijerink that *the emission around 585 ns has contributions from ZnS trap states and that the* Mn^{2+} *emission lifetime is not different from that of the bulk.*[49] These results help to resolve the controversy in the literature regarding the lifetime of the Mn^{2+} emission in Mn-doped ZnS nanoparticles.

Metal Oxide Nanoparticles: TiO_2, SnO_2, Fe_2O_3, and ZnO. Metal oxides play an important role in catalysis and photocatalysis and as paint pigments. Their nanoparticles can usually be prepared easily by hydrolysis. Among the different metal oxide nanoparticles studied, TiO_2 has received the most attention because of its stability, easy availability, and promise for applications, e.g., solar energy conversion.[26] Studies of charge carrier dynamics have been performed for TiO_2 nanoparticles alone and, more popularly, with dye sensitization. For TiO_2 NPs alone with excitation at 310 nm, the photoinduced electrons were found to decay following second-order kinetics with a second-order recombination rate constant of 1.8×10^{-10} cm^3/s.[155] The electron trapping was suggested to occur on the time scale of 180 fs.[112]

Dye sensitization of TiO_2 has been studied extensively, primarily because of its potential use for solar energy conversion[26] and photocatalysis.[156] Since TiO_2 alone does not absorb visible light, dye sensitization helps to extend the absorption into the visible region. In dye sensitization, the electron is injected from a dye molecule on the TiO_2 nanoparticle surface, as illustrated in the top of Figure 9. There are several requirements for this to work effectively. First, the excited state of the dye molecule needs to lie above the bottom of the conduction band of the TiO_2 nanoparticle. Second, strong binding of the dye onto the TiO_2 nanoparticle surface is desired

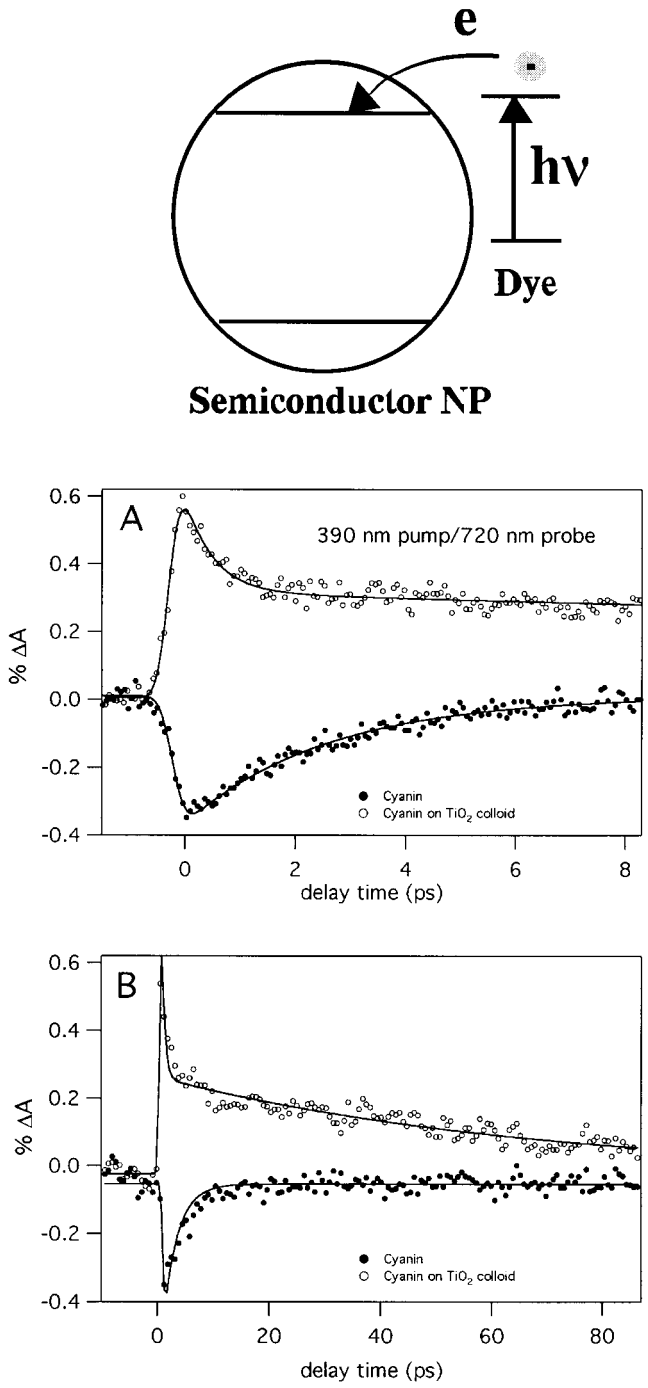

Figure 9. Top: Schematic illustration of charge injection in dye sensitization of a semiconductor NP. Middle and Bottom: transient decay profiles of photoinduced electron transfer from an anthocyanin dye molecule to TiO_2 NPs on a short (middle) and long (bottom) time scale probed at 780 nm following excitation at 390 nm.

for fast and efficient injection. Third, back electron transfer to the dye cation following injection should be minimal. Fourth, the dye molecule must have strong absorption in the visible region of spectrum for solar energy conversion. A number of dye molecules have been studied and tested for solar energy conversion applications over the years.[157] To date, the dye molecule that shows most promise for applications is a Ru complex, Ru(4,4′-dicarboxyl-2,2′-bipyridine)$_2$ $(NCS)_2$ (N3), which showed the highest reported light-to-electricity conversion efficiency of 10%.[26,158] This work has stimulated strong interest in understanding the mechanism of charge injection and recombination in such dye-sensitized nanocrytalline systems.

The rates of electron injection and subsequent recombination or back electron transfer in dye sensitization are expected to depend on the nature of the dye molecule and the NPs, especially the surface characteristics of the NPs. The interaction between the dye and the NP surface will determine the rates and yields of forward as well as reverse electron transfer.[7,12] The shape (facets) and size of the particles could also be important and tend to vary from sample to sample, depending on the preparation methods used. Recent studies of the injection rate have found that electron injection (forward electron transfer) is generally extremely fast, ~100 fs. For instance, for the coumarin 343 dye on TiO_2, the electron injection rate was found to be around 200 fs.[159] For the N_3 dye on TiO_2, the first direct fs measurement reported a hot electron injection time of <25 fs.[160] However, there has been some debate over possible degradation of the dye sample used.[161,162] A picosecond infrared study showed an upper limit of 20 ps for the electron injection time.[163] More recent work by Ellingson et al. on N_3 on TiO_2 reported an injection time of <50 fs based on transient infrared measurements.[164] We have recently studied an anthocyanin dye adsorbed on TiO_2 NPs and found an electron injection time of <100 fs.[165] The assignment is made simple in this system since the dye alone has a stimulated emission signal (similar to a transient bleach), while the dye on TiO_2 has a transient absorption signal. By carefully performing several control experiments, we were able to unambiguously assign the transient absorption signal to electrons injected into TiO_2, which has a rise time of <100 fs. As shown in the bottom panels of Figure 9, a positive transient absorption signal was observed only when the dye is adsorbed onto TiO_2 NPs while the dye alone or on ZrO_2 or complexing with Al^{3+} ions showed a negative signal that is a result of bleach or stimulated emission.[61] This unequivocally establishes that the electron injection from the excited dye molecule to the TiO_2 NP takes place in <100 fs. While forward electron transfer has generally been found to be very fast, back electron transfer was found to occur on a range of time scales, from about 10 ps to μs, depending on the nature of the dye and the nanoparticle.[17,165,166] For example, both forward and reverse electron transfer have been studied in the case of anthracenecarboxylic acids adsorbed on different types of TiO_2 NPs and were found to be dependent on the dye molecular structure and the method used to synthesize the TiO_2 particles.[166]

For SnO_2 NPs, most dynamics work has also focused on dye sensitization.[167−169] For instance, fs transient absorption and bleach studies have been performed on cresyl violet H-aggregate dimers adsorbed on SnO_2 colloidal particles.[169] It was found that the electron injection from the higher energy state, resulting from exciton splitting, of the dimer to SnO_2 NPs occurs in <100 fs and back electron transfer occurs with a 12 ps time constant.

Another intriguing metal oxide system is iron oxide (Fe_2O_3). Fe_2O_3 can exist in the γ phase (maghemite) or α phase (hematite). In its α phase it can be used as a photocatalyst and in its γ phase it can be used as a component in magnetic recording media because of its magnetic properties.[60,62,170−172] We have recently carried out fs dynamics studies of electronic relaxation in both γ and α phased Fe_2O_3 nanoparticles with 390 nm excitation. The relaxation dynamics were found to be very similar between the two types of nanoparticles, despite their difference in magnetic properties and particle shape: γ being mostly spherical and α being mostly spindle-shaped (Figure 1C).[61] The relaxation featured a multiexponential decay with time constants of 0.36, 4.2, and 67 ps. The overall fast relaxation, in conjunction with very weak fluorescence, indicates extremely efficient nonradiative decay processes, possibly related to the intrinsic dense band structure or a high density of trap states. The fast relaxation of the photoinduced electrons is consistent with the typically low photocurrent efficiency of Fe_2O_3 electrodes, since the short lifetime due to fast electron−hole recombination does not favor charge transport that is necessary for photocurrent generation.[61]

Similar studies have been done on other metal oxides such as ZnO. For ZnO NPs with 310 nm excitation, the photoinduced electron decay was found to follow second-order kinetics,[173] similar to TiO_2.[155] It was also found that the initial electron trapping and subsequent recombination dynamics were size dependent. The trapping rate was found to increase with increasing particle size, which was explained with a trap-to-trap hopping mechanism. The electron−hole recombination is faster and occurs to a greater extent in larger particles because there are two different types of trap states. A different explanation, based on exciton−exciton annihilation upon trap state saturation, has been recently proposed by us for similar excitation intensity dependent and size dependent relaxation observed in CdS and CdSe NPs.[46] This explanation would also seem to be consistent with the results observed for TiO_2[155] and ZnO.[173]

Silver Halides (AgI and AgBr) Nanoparticles. Silver halide nanoparticles play an important role in photography, and their synthesis is relatively simple. We have recently investigated the ultrafast charge carrier dynamics in AgI and core/shell structured AgI/Ag_2S and ArBr/Ag_2S NPs.[68] It was found that the electronic relaxation of AgI follows a double exponential decay with time constants of 2.5 ps and >0.5 ns, which are independent of excitation intensity at 390 nm. The fast decay was attributed to trapping and nonradiative electron−hole recombination dominated by a high density of trap states, as indicated by extremely low luminescence. The slow decay was assigned to reaction of deep trapped electrons with silver cations to form silver (Ag) atom, which is the basis for latent image formation in photography. The slow decay agrees with early nanosecond studies.[174] When we compared two core/shell systems, AgI/Ag_2S and AgBr/Ag_2S, we observed a new 4 ps rise component with AgBr/Ag_2S. This was taken as an indication of electron transfer from Ag_2S to AgBr.[68] At the time of experiments, we were unable to make pure Ag_2S nanoparticles. However, very recently we have succeeded in synthesizing pure Ag_2S nanoparticles capped with cysteine and glutathione. The dynamics observed for pure Ag_2S NPs are very similar to that of the core/shell structured AgBr/Ag_2S.[56] Therefore, the 4 ps rise feature attributed to electron transfer previously is most likely incorrect. A more likely explanation is that the rise is due to contribution from a transient bleach signal, since there is noticeable ground-state absorption at the probe wavelength. Other supporting evidence of this new assignment has been found in our most recent study of neat Ag_2S NPs.[56] Even though we need to change the assignment of the 4 ps rise for Ag_2S/AgBr, the original assignment for the AgI and AgI/Ag_2S NPs should still be valid.

Silicon (Si) Nanoparticles. Silicon NPs have attracted considerable attention recently because of their luminescence properties. Since bulk silicon is an indirect band gap semiconductor with a band gap of 1.1 eV, it is very weakly luminescent. For optoelectronics applications, it is highly desirable to develop luminescent materials that are compatible with the current existing silicon technology developed and matured for the electronics industry. The weak luminescence of bulk silicon presents a major obstacle to its use for the fast-growing

optoelectronics industry. The discovery in 1990[175] that porous and nanocrystalline Si emit visible light with high quantum yield has raised hopes for new photonic devices based on silicon and stimulated strong research interest in porous silicon and Si nanoparticles.[75−78,176−178] Various methods have been used to make Si nanoparticles, including slow combustion of silane,[176] reduction of $SiCl_4$ by Na,[31] separation from porous Si following HF acid electrochemical etching,[71−73] microwave discharge,[74] laser vaporization/controlled condensation,[75] high-pressure aerosol reaction,[76] laser-induced chemical vapor deposition,[77] and chemical vapor deposition.[78] Si NPs are difficult to make using wet colloidal chemistry techniques. We have performed preliminary fs studies of charge carrier dynamics in Si nanoparticles made by electrochemical etching[73] and found that the relaxation time is a few picoseconds and the lifetime is longer for particles with higher luminescence yield. A recent dynamics study on ion-implanted Si nanocrystals using femtosecond transient absorption identified two photoinduced absorption features, attributed to charge carriers in nanocrystal quantized states with higher energy and faster relaxation and Si/SiO_2 interface states with lower energy and slower relaxation.[179] Red emission observed in this sample was shown to be from surface trap states and not from quantized states. The faster relaxation of the blue emission relative to that of the red emission is similar to that observed for CdS NPs.[46]

Nanoparticles of Layered Semiconductors: MoS_2, PbI_2, and BiI_3. Layered semiconductors such as PbI_2 and MoS_2 form an interesting class of semiconductors with some unique properties.[180] Nanoparticles of layered semiconductor can be prepared using techniques similar to those used for other semiconductors. Some can be made by simply dissolving bulk crystals in suitable solvents. Dynamic studies of layered semiconductor NPs have been limited. A picosecond transient absorption study of charge carrier relaxation in MoS_2 NPs has been reported,[181] and the relaxation was found to be dominated by trap states. The relaxation from shallow traps to deep traps is fast (40 ps) at room temperature and slows down to 200 ps at 20 K.

We have very recently conducted a fs study of charge carrier relaxation dynamics in PbI_2 nanoparticles and found that the relaxation was dominated by surface properties and independent of particle size in the size range (3−100 nm) studied.[65] The relaxation was found to be strongly dependent on the solvent used. The early time dynamics were found to show some signs of oscillation with a period varying with solvent but not with size. As shown in Figure 10, the period is 6 ps in acetonitrile. In alcohol solvents, the period is 1.7 ps. The exact origin of the oscillation is not completely clear at this point, and such features are rarely observed for colloidal semiconductor NPs. There is a small possibility that the oscillation is related to quantum beats, however, further study is necessary to establish this. On longer time scales, the relaxation was dominated by a 75 ps decay in acetonitrile, while in alcohol solvents, in addition to a 75 ps decay, a fast 6 ps decay was observed. The relaxation in aqueous PVA solution featured a double exponential decay with time constants of 1 and 40 ps.[65] The decays have been attributed to trapping and recombination mediated by trap states.

There have been some controversies over the nature of the optical absorption spectrum (Figure 10A), whether it is from PbI_2 nanoparticles or from some kind of iodine complexes, and if the three major absorption peaks are due to different sized "magic" numbered particles.[64,180,182] We have addressed these two questions in detail.[65] Our studies have found no evidence for "magic" numbered particles of different size correlating with

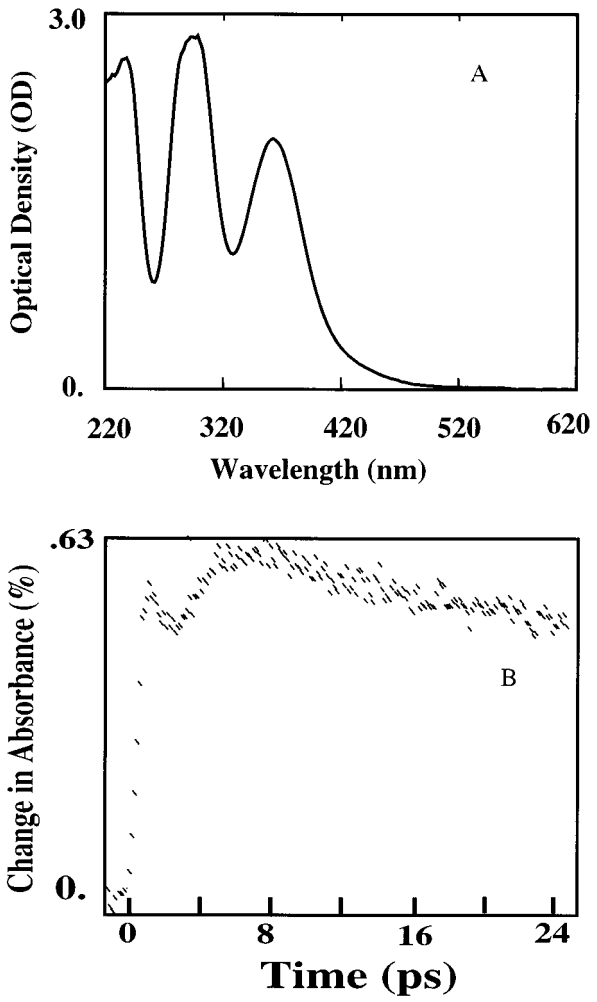

Figure 10. Electronic absorption spectrum (top) and photoinduced electron relaxation dynamics (bottom) of PbI_2 NPs in acetonitrile on a short time scale. The dynamics data, collected with probing at 720 nm and excitation at 390 nm, show what appears to be an oscillation at early times with a period of 6 ps.

the three absorption peaks, and the optical absorption seemed to be dominated by PbI_2 NPs. Using a particle-in-a-rectangular-box model, we can explain the peak positions and the observed blue shift of the peaks with simultaneous decrease in particle size upon aging under light.[69] TEM images and optical studies led us to suggest that that in the photodecomposition process the initially formed large, single-layered particles break down into smaller, multilayered particles, resulting in significant increase in the optical absorption intensity in the visible region and slight blue shift of the absorption peaks.[69]

To get a better understanding of some of the observed features in PbI_2 nanoparticles, we have very recently conducted a comparative study on a similar layered semiconductor, bismuth iodide, BiI_3. The crystal structure of BiI_3 is very similar to that of lead iodide except that one-third of the Pb^{2+} sites are vacant for BiI_3 due to its rhombohedral structure with a layer of metal sandwiched between two hexagonally closed packed layers of iodine.[183] BiI_3 is promising for non-silver based and thermally controlled photographic applications.[184] The band gap of bulk BiI_3 has been reported as 2.1 eV.[185] Bulk layered BiI_3 single crystals show different types of excitonic transitions near the fundamental absorption edge, including direct and indirect excitonic bands and a series of sharp absorption bands due to stacking faults in the crystals.[186,187] Colloidal BiI_3 nanoparticles and BiI_3 clusters in geolite LTA have been synthesized and the

quantum confinement effect has been studied spectroscopically.[183,188,189]

The BiI_3 nanoparticles used in our dynamics studies were prepared using a procedure similar to that for PbI_2 in different solvents, including ethanol, 1-butanol, acetonitrile, water, and aqueous poly(vinyl alcohol) (PVA) matrix as well as in inverse micelles.[69] The particle sizes and shapes were determined using low- and high-resolution transmission electron microscopy. Similar to PbI_2, using a particle-in-a-rectangular-box model, we can explain the peak positions and the blue shift of the peaks with simultaneous decrease in particle size in BiI_3 NPs. With excitation at 390 nm and probing in the visible to near-infrared region, the electronic relaxation dynamics in BiI_3 nanoparticles were directly monitored and found to be similar to that of PbI_2, i.e., sensitive to solvent and insensitive to particle size, and the dynamics observed were somewhat dependent on the probe wavelength and independent of the excitation intensity. In acetonitrile the relaxation was dominated by a 50 ps decay and a long-lived component of 1.3 ns. In alcohol solvents, in addition to a 50 ps decay, a fast 9 ps decay was observed. There appear to be oscillations at early times with a period changing with solvent (5 ps in acetonitrile, 1.3 ps in 1-butanol) but not with particle size, similar to that found for PbI_2 nanoparticles. These oscillations seem to be the characteristics of these layered iodide semiconductor systems. For BiI_3, however, the oscillation periods were slightly shorter and overall relaxation was somewhat faster than that in PbI_2. The decay was much faster in aqueous PVA (9 ps) and in inverse micelles (1.2 and 33 ps) with no oscillations observed. The results suggest that the surface plays a major role in the electronic relaxation process of BiI_3 nanoparticles, just as in PbI_2 nanoparticles, as indicated by the strong solvent dependence. Similar to PbI_2, the influence of particle size is relatively minor in the size range studied (2−100 nm), probably because the relaxation is dominated by surface characteristics that do not vary significantly with size and/or the size is much larger than the exciton Bohr radius (0.61 nm for bulk BiI_3)[189] and thereby spatial confinement is not significant in affecting the relaxation process.

Effects of Particle Surface, Size, and Shape. The examples discussed above seem to suggest that electronic relaxation in semiconductor nanoparticles is dominated by surface properties. This is largely because a high density of surface and defect trap states lies within the band gap and acts to trap photogenerated charge carriers (electrons and holes). These states are usually not observed in optical absorption but in photoluminescence or dynamics measurements that are sensitive to charge carriers in trap states. The density and distribution of trap states are strongly dependent on the nature of the NPs. For example, exciton−exciton annihilation due to trap state saturation has been observed only for some NPs such as CdS, CdSe, TiO_2, and ZnO[46,155] but not for other NPs such as AgI,[68] Fe_2O_3,[61] PbS,[83] and PbI_2.[65] The absence of exciton−exciton annihilation in the latter systems is attributed to a higher density of trap states and thereby a higher threshold of trap state saturation. This explanation is consistent with the very weak fluorescence from these NPs, which indicates a high density of trap states. Interestingly, trap state saturation is also reflected in increased transient absorption over bleach with increasing excitation intensity as in Ag_2S[56] and CuS.[53] Due to difficulty in preparing single sized, single-shaped particles with uniform and well-defined surface properties, there have been no systematic studies on the effects of particle size and shape on the electronic relaxation dynamics. All of the results reported to date seem to indicate a predominant effect of the surface. Therefore, to study the intrinsic size or shape effect, the surface needs to be better controlled, which is possible but usually challenging to do in most cases.

Given these challenges, however, many interesting optical and electronic properties of semiconductor nanoparticles have been unraveled from comparative studies of relatively high quality samples. Furthermore, for many applications, e.g., the nanocrystalline solar cells mentioned earlier or photocatalysis, it is not always necessary to use particles all with the same size, shape, and surface properties. In addition, for surface chemistry applications such as catalysis, the surface states are highly reactive and often necessary for chemical reactions on the surface. Therefore, surface states can be useful or harmful, depending on the nature of the applications of interest. For fundamental understanding of the effects of these parameters, however, it is highly desirable to synthesize particles with well controlled size, shape, and surface characteristics and/or to develop characterization techniques that allow investigation of single particles.[190−193]

Summary and Prospects

Nanoparticles show great promise for a number of emerging technological applications because of their novel properties. To control particle size, shape, and surface properties presents an interesting challenge in the synthesis of nanoparticles. It is these variables that make NPs interesting for studying many fundamental issues related to quantum size effects and interfaces. For applications, one of the major limitations with NPs is that charge transport between particles is very limited compared to bulk single crystalline materials. Thus, it is important to understand interaction between particles, e.g., in superlattice structure, that is critically related to charge transport. The study of interparticle interactions has received growing attention recently. Some alternative systems include nanowires, nanotubes, or nanorods that have enhanced charge transport properties compared to nanoparticles, and they are becoming the subject of active research.

In terms of characterization techniques, surface-sensitive methods are needed to better characterize the surface properties of NPs. It would be highly desirable to develop single particle characterization techniques based on spectroscopy or microscopy or both. This would eliminate the need to prepare single-sized or truly monodisperse particles, which is often difficult to do. There have been some encouraging preliminary reports on spectroscopic studies of single nanoparticles.[190−194] However, dynamics studies of single nanoparticles on the ultrafast time scales have not been reported. Even for single particles, only when the surface properties are better controlled, can the intrinsic size and shape effects be effectively studied, since, otherwise, the surface properties will dominate the optical and electronic properties of the NPs.

Applications of NPs are yet to be fully explored. Some areas of current or potential application include light-emitting diodes, solar cells, lasers, sensors, biological fluorescence imaging, and detectors. Nanocomposite materials of inorganic semiconductor NPs with organic materials or biological molecules, such as conjugated polymers or proteins, are another interesting class of materials worth exploring for both fundamental studies and new technological applications. Such composite materials may take advantage of the useful properties of both the inorganic NPs and the organic or biological materials when properly combined. The interfaces between these different materials are complex and interesting. The possibilities of applications as well as interesting issues concerning nanomaterials are tremendous, and further research and exploration are needed before their full potential is realized.

Acknowledgment. This work was supported in part by grants from the Petroleum Research Fund administered by the American Chemical Society, Collaborative University of California/Los Alamos Research Fund, University of California Energy Institute, University of California Santa Cruz Faculty Research Fund, the Materials Research Institute of Lawrence Livermore National Labs, and the California Energy Commission. I am grateful to people who have contributed to the work described in this paper, including my postdoctors and students, Dr. N. J. Cherepy, Dr. T. W. Roberti, B. A. Smith, A. Sengupta, F. Wu, M. C. Brelle, and collaborators, Dr. K. C. Mandal, Prof. H. Deng, B. Jiang, L. Nguyen, Prof. M. Gratzel, Dr. G. Smestad, Dr. J. Liu, Dr. A. Joly, Dr. Y. Yang, Dr. C. L. Torres-Martinez, Prof. J. L. Coffer, Prof. S. H. Risbud, and Prof. R. K. Mehra.

References and Notes

(1) Efros, A. L.; Efros, A. L. *Fizika i Tekhnika Poluprovodnikov* **1982**, *16*, 1209 [*Sov. Phys. Semicond.* **1982**, *16*, 772].
(2) Brus, L. E. *J. Chem. Phys.* **1984**, *80*, 4403.
(3) Ekimov, A. I.; Efros, A. L.; Ivanov, M. G.; Onushchenko, A. A.; Shumilov, S. K. *Solid State Commun.* **1985**, *56*, 921.
(4) Alivisatos, A. P.; Harris, A. L.; Levinos, N. J.; Steigerwald, M. L.; Brus, L. E. *J. Chem. Phys.* **1988**, *89*, 4001.
(5) Ekimov, A. I.; Efros, A. L.; Ivanov, M. G.; Onushchenko, A. A.; Shumilov, S. K. *Solid State Commun.* **1989**, *69*, 565.
(6) Henglein, A. *Chem. Rev.* **1989**, *89*, 1861−1873.
(7) Gratzel, M. *Heterogeneous Photochemical Electron Transfer*; CRC Press: Boca Raton, 1989.
(8) Bawendi, M. G.; Steigerwald, M. L.; Brus, L. E. *Annu. Rev. Phys. Chem.* **1990**, *41*, 477.
(9) Bawendi, M. G.; Wilson, W. L.; Rothberg, L.; Carroll, P. J.; Jedju, T. M.; Steigerwald, M. L.; Brus, L. E. *Phys. Rev. Lett.* **1990**, *65*, 1623.
(10) Wang, Y. *Acc. Chem. Res.* **1991**, *24*, 133.
(11) Tolbert, S. H.; Alivisatos, A. P. *Annu. Rev. Phys. Chem.* **1995**, *46*, 595.
(12) *Surface Electron-Transfer Processes*; Miller, R. J. D., McLendon, G. L., Nozik, A. J., Schmickler, W., Willig, F., Eds.; VCH: New York, 1995; p 167.
(13) Fendler, J. H.; Meldrum, F. C. *Adv. Mater.* **1995**, *7*, 607.
(14) Alivisatos, A. P. *J. Phys. Chem.* **1996**, *100*, 13226.
(15) Alivisatos, A. P. *Science* **1996**, *271*, 933.
(16) Liu, J.; Feng, X. D.; Fryxell, G. E.; Wang, L. Q.; Kim, A. Y.; Gong, M. L. *Adv. Mater.* **1998**, *10*, 161.
(17) Kamat, P. V. *Prog. Inorg. Chem.* **1997**, *44*, 273.
(18) Zhang, J. Z. *Acc. Chem. Res.* **1997**, *30*, 423.
(19) Collier, C. P.; Vossmeyer, T.; Heath, J. R. *Annu. Rev. Phys. Chem.* **1998**, *49*, 371.
(20) Heath, J. R.; Shiang, J. J. *Chem. Soc. Rev.* **1998**, *27*, 65.
(21) Schmitt-Rink, S.; Miller, D. A. B.; Chemla, D. S. *Phys. Rev. B: Condens. Matter* **1987**, *35*, 8113.
(22) Goldstein, A. N.; Echer, C. M.; Alivisatos, A. P. *Science* **1992**, *256*, 1425.
(23) Tolbert, S. H.; Alivisatos, A. P. *Science* **1994**, *265*, 373.
(24) Feldheim, D. L.; Keating, C. D. *Chem. Soc. Rev.* **1998**, *27*, 1.
(25) Schlamp, M. C.; Peng, X. G.; Alivisatos, A. P. *J. Appl. Phys.* **1997**, *82*, 5837.
(26) O'Regan, B.; Gratzel, M. *Nature* **1991**, *353*, 737.
(27) Nayral, C.; Ould-Ely, T.; Maisonnat, A.; Chaudret, B.; Fau, P.; Lescouzeres, L.; Peyre-Lavigne, A. *Adv. Mater.* **1999**, *11*, 61.
(28) Bruchez, M.; Moronne, M.; Gin, P.; Weiss, S.; Alivisatos, A. P. *Science* **1998**, *281*, 2013.
(29) Chan, W. C. W.; Nie, S. M. *Science* **1998**, *281*, 2016.
(30) Xia, Y. N.; Rogers, J. A.; Paul, K. E.; Whitesides, G. M. *Chem. Rev.* **1999**, *99*, 1823.
(31) Heath, J. R. *Science* **1992**, *258*, 1131.
(32) Weller, H. *Angew. Chem., Int. Ed. Engl.* **1996**, *35*, 1079.
(33) Andres, R. P.; Bielefeld, J. D.; Henderson, J. I.; Janes, D. B.; Kolagunta, V. R.; Kubiak, C. P.; Mahoney, W. J.; Osifchin, R. G. *Science* **1996**, *273*, 1690.
(34) Alivisatos, A. P. *Endeavour* **1997**, *21*, 56.
(35) Sarathy, K. V.; Thomas, P. J.; Kulkarni, G. U.; Rao, C. N. R. *J. Phys. Chem. B* **1999**, *103*, 399.
(36) Spanhel, L.; Haase, M.; Weller, H.; Henglein, A. *J. Am. Chem. Soc.* **1987**, *109*, 5649.
(37) Gallardo, S.; Gutierrez, M.; Henglein, A.; Janata, E. *Ber. Bunsen-Ges. Phys. Chem.* **1989**, *93*, 1080.
(38) O'Neil, M.; Marohn, J.; McLendon, G. *Chem. Phys. Lett.* **1990**, *168*, 208.
(39) O'Neil, M.; Marohn, J.; McLendon, G. *J. Phys. Chem.* **1990**, *94*, 4356.
(40) Colvin, V. L.; Goldstein, A. N.; Alivisatos, A. P. *J. Am. Chem. Soc.* **1992**, *114*, 5221.
(41) Duonghong, D.; Ramsden, J. J.; Gratzel, M. *J. Am. Chem. Soc.* **1982**, *104*, 2977.
(42) Murray, C. B.; Norris, D. J.; Bawendi, M. G. *J. Am. Chem. Soc.* **1993**, *115*, 8706.
(43) Katari, J. E. B.; Colvin, V. L.; Alivisatos, A. P. *J. Phys. Chem.* **1994**, *98*, 4109.
(44) Bae, W.; Mehra, R. K. *J. Inorg. Biochem.* **1998**, *70*, 125.
(45) Nguyen, L.; Kho, R.; Bae, W.; Mehra, R. K. *Chemosphere* **1998**, *38*, 155.
(46) Roberti, T. W.; Cherepy, N. J.; Zhang, J. Z. *J. Chem. Phys.* **1998**, *108*, 2143.
(47) Rogach, A. L.; Kornowski, A.; Gao, M. Y.; Eychmuller, A.; Weller, H. *J. Phys. Chem. B* **1999**, *103*, 3065.
(48) Khosravi, A. A.; Kundu, M.; Jatwa, L.; Deshpande, S. K.; Bhagwat, U. A.; Sastry, M.; Kulkarni, S. K. *Appl. Phys. Lett.* **1995**, *67*, 2702.
(49) Smith, B. A.; Zhang, J. Z.; Joly, A.; Liu, J. *Phys. Rev. B*, in press.
(50) Nenadovic, M. T.; Comor, M. I.; Vasic, V.; Micic, O. I. *J. Phys. Chem.* **1990**, *94*, 6390.
(51) Zhou, H. S.; Honma, I.; Komiyama, H.; Haus, J. W. *J. Phys. Chem.* **1993**, *97*, 895.
(52) Silvester, E. J.; Grieser, F.; Sexton, B. A.; Healy, T. W. *Langmuir* **1991**, *7*, 2917.
(53) Brelle, M. C.; Torres-Martinez, C. L.; McNulty, J. C.; Mehra, R. K.; Zhang, J. Z. *Pure Appl. Chem.* **2000**, *72*, 101.
(54) Wilcoxon, J. P.; Samara, G. A. *Phys. Rev. B: Condens. Matter* **1995**, *51*, 7299.
(55) Parsapour, F.; Kelley, D. F.; Craft, S.; Wilcoxon, J. P. *J. Chem. Phys.* **1996**, *104*, 4978.
(56) Brelle, M. C.; Zhang, J. Z.; Nguyen, L.; Mehra, R. K. *J. Phys. Chem. A* **1999**, *103*, 10194.
(57) Serpone, N.; Lawless, D.; Khairutdinov, R. *J. Phys. Chem.* **1995**, *99*, 16646.
(58) Choi, W. Y.; Termin, A.; Hoffmann, M. R. *J. Phys. Chem.* **1994**, *98*, 13669−13679.
(59) Smith, B. A.; Waters, D. A.; Faulhaber, A. E.; Kreger, M.; Zhang, J. Z. *J. Sol-Gel Sci. Technol.* **1997**, *9*, 125.
(60) Kang, Y. S.; Risbud, S.; Rabolt, J. F.; Stroeve, P. *Chem. Mater.* **1996**, *8*, 2209.
(61) Cherepy, N. J.; Liston, D. B.; Lovejoy, J. A.; Deng, H. M.; Zhang, J. Z. *J. Phys. Chem. B* **1998**, *102*, 770.
(62) Faust, B. C.; Hoffmann, M. R.; Bahnemann, D. W. *J. Phys. Chem.* **1989**, *93*, 6371.
(63) Spanhel, L.; Anderson, M. A. *J. Am. Chem. Soc.* **1991**, *113*, 2826.
(64) Sandroff, C. J.; Hwang, D. M.; Chung, W. M. *Phys. Rev. B: Condens. Matter* **1986**, *33*, 5953.
(65) Sengupta, A.; Jiang, B.; Mandal, K. C.; Zhang, J. Z. *J. Phys. Chem. B* **1999**, *103*, 3128.
(66) Artemyev, M. V.; Rakovich, Y. P.; Yablonski, G. P. *J. Cryst. Growth* **1997**, *171*, 447.
(67) Henglein, A.; Gutierrez, M.; Weller, H.; Fojtik, A.; Jirkovsky, J. *Ber. Bunsen-Ges. Phys. Chem.* **1989**, *93*, 593.
(68) Brelle, M. C.; Zhang, J. Z. *J. Chem. Phys.* **1998**, *108*, 3119.
(69) Sengupta, A.; Mandal, K. C.; Zhang, J. Z. *J. Phys. Chem. B*, in press.
(70) Fojtik, A.; Weller, H.; Fiechter, S.; Henglein, A. *Chem. Phys. Lett.* **1987**, *134*, 477.
(71) Heinrich, J. L.; Curtis, C. L.; Credo, G. M.; Kavanagh, K. L.; Sailor, M. J. *Science* **1992**, *255*, 66.
(72) Bley, R. A.; Kauzlarich, S. M.; Davis, J. E.; Lee, H. W. H. *Chem. Mater.* **1996**, *8*, 1881.
(73) Zhang, L. B.; Coffer, J. L.; Zerda, T. W. *J. Sol-Gel Sci. Technol.* **1998**, *11*, 267.
(74) Takagi, H.; Ogawa, H.; Yamazaki, Y.; Ishizaki, A.; Nakagiri, T. *Appl. Phys. Lett.* **1990**, *56*, 2379.
(75) Li, S. T.; Silvers, S. J.; ElShall, M. S. *J. Phys. Chem. B* **1997**, *101*, 1794.
(76) Littau, K. A.; Szajowski, P. J.; Muller, A. J.; Kortan, A. R.; Brus, L. E. *J. Phys. Chem.* **1993**, *97*, 1224.
(77) Wang, W. X.; Liu, S. H.; Zhang, Y.; Mei, Y. B.; Chen, K. X. *Physica B* **1996**, *225*, 137.
(78) Cao, W. Q.; Hunt, A. J. *Appl. Phys. Lett.* **1994**, *64*, 2376.
(79) Reetz, M. T.; Helbig, W.; Quaiser, S. A.; Stimming, U.; Breuer, N.; Vogel, R. *Science* **1995**, *267*, 367.
(80) Chestnoy, N.; Harris, T. D.; Hull, R.; Brus, L. E. *J. Phys. Chem.* **1986**, *90*, 3393.
(81) Petroski, J. M.; Wang, Z. L.; Green, T. C.; El-Sayed, M. A. *J. Phys. Chem. B* **1998**, *102*, 3316.

(82) Link, S.; Mohamed, M. B.; El-Sayed, M. A. *J. Phys. Chem. B* **1999**, *103*, 3073.
(83) Patel, A.; Wu, F.; Zhang, J. Z.; Torres-Marinez, C. L.; Mehra, R. K.; Yang, Y.; Risbud, S. H. *J. Phys. Chem. B*, submitted.
(84) Weller, H.; Schmidt, H. M.; Koch, U.; Fojtik, A.; Baral, S.; Henglein, A.; Kunath, W.; Weiss, K.; Dieman, E. *Chem. Phys. Lett.* **1986**, *124*, 557.
(85) Zhang, J. Z.; O'Neil, R. H.; Roberti, T. W. *J. Phys. Chem.* **1994**, *98*, 3859.
(86) Herron, N.; Calabrese, J. C.; Farneth, W. E.; Wang, Y. *Science* **1993**, *259*, 1426.
(87) Lee, G. S. H.; Craig, D. C.; Ma, I.; Scudder, M. L.; Bailey, T. D.; Dance, I. G. *J. Am. Chem. Soc.* **1988**, *110*, 4863.
(88) Vossmeyer, T.; Reck, G.; Katsikas, L.; Haupt, E. T. K.; Schulz, B.; Weller, H. *Inorg. Chem.* **1995**, *34*, 4926.
(89) vanBuuren, T.; Dinh, L. N.; Chase, L. L.; Siekhaus, W. J.; Terminello, L. J. *Phys. Rev. Lett.* **1998**, *80*, 3803.
(90) Chen, L. X.; Rajh, T.; Wang, Z. Y.; Thurnauer, M. C. *J. Phys. Chem. B* **1997**, *101*, 10688.
(91) Rockenberger, J.; Troger, L.; Rogach, A. L.; Tischer, M.; Grundmann, M.; Eychmuller, A.; Weller, H. *J. Chem. Phys.* **1998**, *108*, 7807.
(92) Ernsting, N. P.; Kaschke, M.; Weller, H.; Katsikas, L. *J. Opt. Soc. Am. B*−*Opt. Phys.* **1990**, *7*, 1630.
(93) Kamalov, V. F.; Little, R.; Logunov, S. L.; El-Sayed, M. A. *J. Phys. Chem.* **1996**, *100*, 6381.
(94) Iwai, S.; Murata, S.; Tachiya, M. *J. Chem. Phys.* **1998**, *109*, 5963.
(95) Dneprovskii, V. S.; Klimov, V. I.; Okorokov, D. K.; Vandyshev, Y. V. *Solid State Commun.* **1992**, *81*, 227.
(96) Pankove, J. I. *Optical Properties in Semiconductors*; Dover Publications: New York, 1971.
(97) Brus, L. *J. Phys. Chem.* **1986**, *90*, 2555.
(98) Evans, J. E.; Springer, K. W.; Zhang, J. Z. *J. Chem. Phys.* **1994**, *101*, 6222.
(99) Dimitrijevic, N. M.; Kamat, P. V. *J. Phys. Chem.* **1987**, *91*, 2096.
(100) Haase, M.; Weller, H.; Henglein, A. *J. Phys. Chem.* **1988**, *92*, 4706.
(101) Hilinski, E. F.; Lucas, P. A.; Ying, W. *J. Chem. Phys.* **1988**, *89*, 3534.
(102) Kamat, P. V.; Dimitrijevic, N. M.; Nozik, A. J. *J. Phys. Chem.* **1989**, *93*, 2873.
(103) Kamat, P. V.; Dimitrijevic, N. M. *J. Phys. Chem.* **1989**, *93*, 4259.
(104) Wang, Y.; Suna, A.; McHugh, J.; Hilinski, E. F.; Lucas, P. A.; Johnson, R. D. *J. Chem. Phys.* **1990**, *92*, 6927.
(105) Vossmeyer, T.; Katsikas, L.; Giersig, M.; Popovic, I. G.; Diesner, K.; Chemseddine, A.; Eychmuller, A.; Weller, H. *J. Phys. Chem.* **1994**, *98*, 7665.
(106) Henglein, A.; Kumar, A.; Janata, E.; Weller, H. *Chem. Phys. Lett.* **1986**, *132*, 133.
(107) Kang, K. I.; Kepner, A. D.; Gaponenko, S. V.; Koch, S. W.; Hu, Y. Z.; Peyghambarian, N. *Phys. Rev. B: Condens. Matter* **1993**, *48*, 15449.
(108) Klimov, V.; Hunsche, S.; Kurz, H. *Phys. Rev. B: Condens. Matter* **1994**, *50*, 8110.
(109) Zhang, J. Z.; Oneil, R. H.; Roberti, T. W.; McGowen, J. L.; Evans, J. E. *Chem. Phys. Lett.* **1994**, *218*, 479.
(110) Zheng, J. P.; Kwok, H. S. *Appl. Phys. Lett.* **1994**, *65*, 1151.
(111) Wu, F.; Zhang, J. Z.; Bretchal, H.; Lounis, B.; Moerner, W. E. *Chem. Phys. Lett.* submitted.
(112) Skinner, D. E.; Colombo, D. P.; Cavaleri, J. J.; Bowman, R. M. *J. Phys. Chem.* **1995**, *99*, 7853.
(113) Mittleman, D. M.; Schoenlein, R. W.; Shiang, J. J.; Colvin, V. L.; Alivisatos, A. P.; Shank, C. V. *Phys. Rev. B: Condens. Matter* **1994**, *49*, 14435.
(114) Klimov, V.; Bolivar, P. H.; Kurz, H. *Phys. Rev. B: Condens. Matter* **1996**, *53*, 1463.
(115) Logunov, S.; Green, T.; Marguet, S.; El-Sayed, M. A. *J. Phys. Chem. A* **1998**, *102*, 5652.
(116) Burda, C.; Green, T. C.; Link, S.; El-Sayed, M. A. *J. Phys. Chem. B* **1999**, *103*, 1783.
(117) Ekimov, A. I.; Hache, F.; Schanneklein, M. C.; Ricard, D.; Flytzanis, C.; Kudryavtsev, I. A.; Yazeva, T. V.; Rodina, A. V.; Efros, A. L. *J. Opt. Soc. Am. B: Opt. Phys.* **1993**, *10*, 100.
(118) Norris, D. J.; Sacra, A.; Murray, C. B.; Bawendi, M. G. *Phys. Rev. Lett.* **1994**, *72*, 2612.
(119) Norris, D. J.; Bawendi, M. G. *Phys. Rev. B: Condens. Matter* **1996**, *53*, 16338.
(120) Brus, L. E.; Efros, A. L.; Itoh, T. *J. Lumin.* **1996**, *70*, R7.
(121) Banin, U.; Lee, C. J.; Guzelian, A. A.; Kadavanich, A. V.; Alivisatos, A. P.; Jaskolski, W.; Bryant, G. W.; Efros, A. L.; Rosen, M. *J. Chem. Phys.* **1998**, *109*, 2306.
(122) Nirmal, M.; Murray, C. B.; Bawendi, M. G. *Phys. Rev. B: Condens. Matter* **1994**, *50*, 2293.
(123) Gao, M. Y.; Yang, Y.; Yang, B.; Shen, J. C.; Ai, X. C. *J. Chem. Soc., Faraday Trans.* **1995**, *91*, 4121.
(124) Schneider, T.; Haase, M.; Kornowski, A.; Naused, S.; Weller, H.; Forster, S.; Antonietti, M. *Ber. Bunsen-Ges. Phys. Chem. Chem. Phys.* **1997**, *101*, 1654.
(125) Ai, X. C.; Guo, L.; Zou, Y. H.; Li, Q. S.; Zhu, H. S. *Mater. Lett.* **1999**, *38*, 131.
(126) Machol, J. L.; Wise, F. W.; Patel, R. C.; Tanner, D. B. *Phys. Rev. B: Condens. Matter* **1993**, *48*, 2819.
(127) Drummond, K. M.; Grieser, F.; Healy, T. W.; Silvester, E. J.; Giersig, M. *Langmuir* **1999**, *15*, 6637.
(128) Gotsis, H. J.; Barnes, A. C.; Strange, P. *J. Phys.: Condens. Matter* **1992**, *4*, 10461.
(129) Grijalva, H.; Inoue, M.; Boggavarapu, S.; Calvert, P. *J. Mater. Chem.* **1996**, *6*, 1157.
(130) Nozaki, H.; Shibata, K.; Ohhashi, N. *J. Solid State Chem.* **1991**, *91*, 306.
(131) Saito, S.; Kishi, H.; Nie, K.; Nakamaru, H.; Wagatsuma, F.; Shinohara, T. *Phys. Rev. B: Condens. Matter* **1997**, *55*, 14527.
(132) Sugiura, C.; Yamasaki, H.; Shoji, T. *J. Phys. Soc. Jpn.* **1994**, *63*, 1172.
(133) Yumashev, K. V.; Prokoshin, P. V.; Malyarevich, A. M.; Mikhailov, V. P.; Artemyev, M. V.; Gurin, V. S. *Appl. Phys. B: Lasers Optics* **1997**, *64*, 73.
(134) Klimov, V.; Bolivar, P. H.; Kurz, H.; Karavanskii, V.; Krasovskii, V.; Korkishko, Y. *Appl. Phys. Lett.* **1995**, *67*, 653.
(135) Grozdanov, I.; Najdoski, M. *J. Solid State Chem.* **1995**, *114*, 469.
(136) Artemyev, M. V.; Gurin, V. S.; Yumashev, K. V.; Prokoshin, P. V.; Maljarevich, A. M. *J. Appl. Phys.* **1996**, *80*, 7028.
(137) Kitova, S.; Eneva, J.; Panov, A.; Haefke, H. *J. Imaging Sci. Technol.* **1994**, *38*, 484.
(138) Motte, L.; Billoudet, F.; Pileni, M. P. *J. Mater. Sci.* **1996**, *31*, 38.
(139) Kennedy, T. A.; Glaser, E. R.; Klein, P. B.; Bhargava, R. N. *Phys. Rev. B: Condens. Matter* **1995**, *52*, 14356.
(140) Igarashi, T.; Isobe, T.; Senna, M. *Phys. Rev. B: Condens. Matter* **1997**, *56*, 6444.
(141) Feltin, N.; Levy, L.; Ingert, D.; Pileni, M. P. *J. Phys. Chem. B* **1999**, *103*, 4.
(142) Counio, G.; Esnouf, S.; Gacoin, T.; Boilot, J. P. *J. Phys. Chem.* **1996**, *100*, 20021.
(143) Bhargava, R. N.; Gallagher, D.; Hong, X.; Nurmikko, A. *Phys. Rev. Lett.* **1994**, *72*, 416.
(144) Bhargava, R. N. *J. Lumin.* **1996**, *70*, 85.
(145) Yu, J. Q.; Liu, H. M.; Wang, Y. Y.; Jia, W. Y. *J. Lumin.* **1998**, *79*, 191.
(146) Pohl, U. W.; Gumlich, H. E. *Phys. Rev. B: Condens. Matter* **1989**, *40*, 1194.
(147) Devisschere, P.; Neyts, K.; Corlatan, D.; Vandenbossche, J.; Barthou, C.; Benalloul, P.; Benoit, J. *J. Lumin.* **1995**, *65*, 211.
(148) Sooklal, K.; Cullum, B. S.; Angel, S. M.; Murphy, C. J. *J. Phys. Chem.* **1996**, *100*, 4551.
(149) Jin, C. M.; Yu, J. Q.; Sun, L. D.; Dou, K.; Hou, S. G.; Zhao, J. L.; Chen, Y. M.; Huang, S. H. *J. Lumin.* **1995**, *66*−*7*, 315.
(150) Curie, D. *R. Acad. Sci.* **1964**, *258*, 3269.
(151) Bol, A. A.; Meijerink, A. *Phys. Rev. B: Condens. Matter* **1998**, *58*, R15997.
(152) Qi, L. M.; Ma, J. M.; Cheng, H. M.; Zhao, Z. G. *Colloids Surf., A* **1996**, *111*, 195.
(153) Cizeron, J.; Pileni, M. P. *J. Phys. Chem. B* **1997**, *101*, 8887.
(154) Rossetti, R.; Hull, R.; Gibson, J. M.; Brus, L. E. *J. Chem. Phys.* **1985**, *82*, 552.
(155) Colombo, D. P.; Roussel, K. A.; Saeh, J.; Skinner, D. E.; Cavaleri, J. J.; Bowman, R. M. *Chem. Phys. Lett.* **1995**, *232*, 207.
(156) *Photocatalysis: Fundamentals and Applications*; Serpone, N., Pelizzetti, E., Eds.; Wiley: New York, 1989.
(157) Kalyanasundaram, K.; Gratzel, M. *Coord. Chem. Rev.* **1998**, *177*, 347.
(158) Nazeeruddin, M. K.; Kay, A.; Rodicio, I.; Humphrybaker, R.; Muller, E.; Liska, P.; Vlachopoulos, N.; Gratzel, M. *J. Am. Chem. Soc.* **1993**, *115*, 6382.
(159) Rehm, J. M.; McLendon, G. L.; Nagasawa, Y.; Yoshihara, K.; Moser, J.; Grätzel, M. *J. Phys. Chem.* **1996**, *100*, 9577.
(160) Hannappel, T.; Burfeindt, B.; Storck, W.; Willig, F. *J. Phys. Chem. B* **1997**, *101*, 6799.
(161) Moser, J. E.; Noukakis, D.; Bach, U.; Tachibana, Y.; Klug, D. R.; Durrant, J. R.; Humphrybaker, R.; Gratzel, M. *J. Phys. Chem. B* **1998**, *102*, 3649.
(162) Hannappel, T.; Zimmermann, C.; Meissner, B.; Burfeindt, B.; Storck, W.; Willig, F. *J. Phys. Chem. B* **1998**, *102*, 3651.
(163) Heimer, T. A.; Heilweil, E. J. *J. Phys. Chem. B* **1997**, *101*, 10990.
(164) Ellingson, R. J.; Asbury, J. B.; Ferrere, S.; Ghosh, H. N.; Sprague, J. R.; Lian, T. Q.; Nozik, A. J. *J. Phys. Chem. B* **1998**, *102*, 6455.
(165) Cherepy, N. J.; Smestad, G. P.; Gratzel, M.; Zhang, J. Z. *J. Phys. Chem. B* **1997**, *101*, 9342.

(166) Martini, I.; Hodak, J. H.; Hartland, G. V. *J. Phys. Chem. B* **1998**, *102*, 9508.
(167) Nasr, C.; Liu, D.; Hotchandani, S.; Kamat, P. V. *J. Phys. Chem.* **1996**, *100*, 11054.
(168) Liu, D.; Fessenden, R. W.; Hug, G. L.; Kamat, P. V. *J. Phys. Chem. B* **1997**, *101*, 2583.
(169) Martini, I.; Hartland, G. V.; Kamat, P. V. *J. Phys. Chem. B* **1997**, *101*, 4826.
(170) Leland, J. K.; Bard, A. J. *J. Phys. Chem.* **1987**, *91*, 5076.
(171) Ziolo, R. F.; Giannelis, E. P.; Weinstein, B. A.; Ohoro, M. P.; Ganguly, B. N.; Mehrotra, V.; Russell, M. W.; Huffman, D. R. *Science* **1992**, *257*, 219.
(172) Cornell, R. M.; Schwertmann, U. *The Iron Oxides*; VCH: New York, 1996.
(173) Cavaleri, J. J.; Skinner, D. E.; Colombo, D. P.; Bowman, R. M. *J. Chem. Phys.* **1995**, *103*, 5378.
(174) Micic, O. I.; Meglic, M.; Lawless, D.; Sharma, D. K.; Serpone, N. *Langmuir* **1990**, *6*, 487.
(175) Canham, L. T. *Appl. Phys. Lett.* **1990**, *57*, 1046.
(176) Fojtik, A.; Henglein, A. *Chem. Phys. Lett.* **1994**, *221*, 363.
(177) Brus, L. *J. Phys. Chem.* **1994**, *98*, 3575.
(178) Zhang, L. B.; Coffer, J. L.; Xu, W.; Zerda, T. W. *Chem. Mater.* **1997**, *9*, 2249.
(179) Klimov, V. I.; Schwarz, C. J.; McBranch, D. W.; White, C. W. *Appl. Phys. Lett.* **1998**, *73*, 2603.
(180) Peterson, M. W.; Nozik, A. J. In *Photoelectrochemistry and Photovoltaics of Layered Semiconductors*; Aruchamy, A., Ed.; Kluwer Academic Publishers: Dordrecht, 1992; p 297.
(181) Doolen, R.; Laitinen, R.; Parsapour, F.; Kelley, D. F. *J. Phys. Chem. B* **1998**, *102*, 3906.
(182) Micic, O. I.; Zongguan, L.; Mills, G.; Sullivan, J. C.; Meisel, D. *J. Phys. Chem.* **1987**, *91*, 6221.
(183) Sandroff, C. J.; Kelty, S. P.; Hwang, D. M. *J. Chem. Phys.* **1986**, *85*, 5337.
(184) Chaudhuri, T. K.; Patra, A. B.; Basu, P. K.; Saraswat, R. S.; Acharya, H. N. *Mater. Lett.* **1989**, *8*, 361.
(185) Karasawa, T.; Kamatsu, T.; Miyata, K.; Iida, T.; Kaifu, Y. *Physica* **1981**, *88*, 1058.
(186) Kamatsu, T.; Kaifu, Y. *J. Phys. Soc. Jpn.* **1976**, *40*, 1062.
(187) Kaifu, Y. *J. Lumin.* **1988**, *42*, 61.
(188) Kamatsu, T.; Karasawa, T.; Akai, I.; Iida, T. *J. Lumin.* **1996**, *70*, 448.
(189) Tang, Z. K.; Nozue, Y.; Goto, T. *J. Phys. Soc. Jpn.* **1992**, *61*, 2943.
(190) Nie, S. M.; Emery, S. R. *Science* **1997**, *275*, 1102.
(191) Klar, T.; Perner, M.; Grosse, S.; vonPlessen, G.; Spirkl, W.; Feldmann, J. *Phys. Rev. Lett.* **1998**, *80*, 4249.
(192) Empedocles, S. A.; Bawendi, M. G. *J. Phys. Chem. B* **1999**, *103*, 1826.
(193) Credo, G. M.; Mason, M. D.; Buratto, S. K. *Appl. Phys. Lett.* **1999**, *74*, 1978.
(194) Empedocles, S. A.; Norris, D. J.; Bawendi, M. G. *Phys. Rev. Lett.* **1996**, *77*, 3873.